Palaeogeography, Palaeoclimatology, Palaeoecology 273 (2009) 302–328

Contents lists available at ScienceDirect

Palaeogeography, Palaeoclimatology, Palaeoecology

journal homepage: www.elsevier.com/locate/palaeo

Paleo-redox conditions during OAE 2 reflected in Demerara Rise sediment geochemistry (ODP Leg 207)

Almut Hetzel [a,*], Michael E. Böttcher [b,c], Ulrich G. Wortmann [d], Hans-Jürgen Brumsack [a]

[a] Institute for Chemistry and Biology of the Marine Environment (ICBM), Carl von Ossietzky University, P.O. Box 2503, D-26111 Oldenburg, Germany
[b] Max Planck Institute for Marine Microbiology, Celsiusstrasse 1, D-28359 Bremen, Germany
[c] Leibniz Institute for Baltic Sea Research Warnemünde, Seestrasse 15, D-18119 Warnemünde, Germany
[d] Department of Geology, University of Toronto, 22 Russel street, Ontario, Canada M5S 3B1

ARTICLE INFO

Article history:
Received 1 December 2007
Received in revised form 8 August 2008
Accepted 3 November 2008

Keywords:
Demerara Rise
Ocean Drilling Program
Leg 207
Trace metals
Oceanic Anoxic Event 2
CTBE
Paleoenvironment
Pyrite
Sulfur isotopes

ABSTRACT

Cretaceous black shales deposited under severe oxygen-depletion are carriers of proxy signals for paleoenvironmental conditions. Using high-resolution patterns of iron and sulfur speciation, stable sulfur isotope discrimination, and trace element enrichment from black shale sequences of Sites 1258 and 1260 we identified alterations of the depositional environment during the Cenomanian/Turonian boundary Event (OAE 2) in the southern North Atlantic (ODP Leg 207, Demerara Rise).

Changes in redox-conditions are suggested by high ratios of reactive to total iron which indicate that pyrite was formed both in the water column and within the sediment. This corresponds to euxinic paleoenvironmental conditions with at least temporarily free dissolved sulfide in the water column, a situation similar to the modern deep Black Sea. In addition, besides fixation of sulfide as iron sulfide, organic matter acted as an important sulfur trap during early diagenesis. Stable sulfur isotope fractionation went through a minimum within the OAE 2 interval indicating enhanced sulfur isotope discrimination during highest burial of organic matter (OM) potentially due to lower burial efficiency of reduced sulfur and/or a higher contributions from the oxidative part of the sulfur cycle (e.g., in the water column or the surface sediments). Elevated Fe/Al and Co/Al values within the Cenomanian/Turonian interval confirm euxinic conditions but, at the same time, require a zone where reducing but non-sulfidic conditions prevail, allowing reductive Fe and Co mobilization in oxygen-depleted nearshore sediments. The existence of an expanded oxygen-minimum-zone (OMZ) is demonstrated by extremely low Mn/Al ratios.

A change in the trace metal (TM) inventory of seawater is postulated from a decline in seawater derived TM enrichment. Because hypoxic or even euxinic environments form an important sink for TM, the enlargement of euxinic depositional areas at the global onset of black shale deposition during OAE 2 have likely led to a drawdown of the seawater TM reservoir.

1. Introduction

In the mid-Cretaceous, several distinct periods of organic-rich black shale deposition appear. The enhanced burial of organic carbon in marine sediments during these so called Oceanic Anoxic Events (OAEs; Schlanger and Jenkyns, 1976) is thought to arise either from enhanced bio-productivity or from intensified preservation of organic matter during anoxic conditions (e.g., Arthur et al., 1987, 1988; Schlanger et al., 1987). The Cenomanian–Turonian Boundary Event (CTBE=OAE 2; ca. 93.5 Ma) is one of the best studied global Oceanic Anoxic Events. It is characterized by a global organic carbon burial episode leading to a positive shift in $\delta^{13}C$ values of organic carbon and carbonate (e.g., Schlanger et al., 1987; Arthur et al., 1988; Gale et al., 1993; Erbacher et al., 2005). As the carbon cycle is tightly coupled to the sulfur cycle, perturbations in the global carbon cycle lead to changes in the seawater sulfur isotopic composition (e.g., Strauss, 1999; Paytan et al., 2004; Wortmann and Chernyavsky, 2007).

During Ocean Drilling Program (ODP) Leg 207, relatively expanded, shallowly buried Cretaceous sediments were recovered from Demerara Rise off Suriname, South America. CTBE black shales on Demerara Rise form part of a thick black shale succession encompassing the Albian to Santonian (Shipboard Scientific Party, 2004). This may be the result of both the paleogeographic setting of Demerara Rise (lacking significant ventilation of bottom-waters prior to the opening of the equatorial Atlantic gateway, which may have taken place in the Campanian; see Friedrich and Erbacher, 2006) and enhanced nutrient influx. The latter may have been evoked by terrestrial runoff and/or

* Corresponding author.
E-mail addresses: almut.hetzel@gmx.de (A. Hetzel), michael.boettcher@io-warnemuende.de (M.E. Böttcher), brumsack@icbm.de (H.-J. Brumsack).

0031-0182/$ – see front matter © 2008 Elsevier B.V. All rights reserved.
doi:10.1016/j.palaeo.2008.11.005

upwelling due to the proximal position of Demerara Rise to the South American landmass.

Cretaceous black shales deposited under severe oxygen-depletion are carriers of proxy signals for paleoenvironmental conditions like varying levels of bottom water dysoxia and/or enhanced surface water productivity. Changes in water column redox conditions lead to responses in the coupled biogeochemical sulfur–carbon–metal cycles and associated sedimentary signal formation. Therefore, distribution patterns of iron and sulfur speciation, sulfur isotope partitioning, and enrichments of redox-sensitive and sulfide forming trace metals provide important paleoenvironmental information on dynamics of biogeochemical element cycles and corresponding water column redox-conditions during black shale deposition. Excess iron contribution to selected Cretaceous Leg 207 black shales due to pyrite formation in a euxinic water column was shown by iron and sulfur speciation analyses, and enhanced organic matter sulfurization was shown to be caused by a limitation of reactive iron to form sulfide minerals (Böttcher et al., 2006).

High enrichments of redox-sensitive elements in organic carbon-rich sediments have been related to anoxic bottom waters. Under reducing conditions these metals may either be precipitated as sulfides, co-precipitated with iron sulfides or bound to organic matter (Brumsack, 1980; Jacobs et al., 1985, 1987; Brumsack, 1989; Breit and Wanty, 1991; Hatch and Leventhal, 1992; Calvert and Pedersen, 1993; Piper, 1994; Nijenhuis et al., 1998). Based on the specific trace metal patterns of coastal upwelling areas and euxinic settings Brumsack (2006) discussed the enrichment of trace metals in Cretaceous black shales attempting to ascertain whether enhanced bio-productivity or widespread stagnation triggered black shale formation.

In the present study, we report on a high-resolution geochemical tracer record for black shale sequences of ODP Leg 207 Sites 1258 and 1260 using distribution patterns of trace element enrichment, iron and sulfur speciation, and stable sulfur isotope discrimination to identify changes in redox-conditions of the depositional environment during OAE 2.

2. Material and methods

2.1. Site description

During ODP Leg 207, sediment cores were drilled on the Demerara Rise in the tropical North Atlantic (Fig. 1). The rise stretches ca. 380 km along the coast off Suriname and reaches a width of ca. 220 km from the shelf break to the northeastern escarpment, where water depths increase sharply from 1000 to more than 4500 m. While most of the plateau lies in shallow water (700 m), the northwest margin forms a gentle ramp reaching water depths of 3000 to 4000 m. The five drill sites (Sites 1257–1261) constitute a depth transect with water depths ranging from 1900 to 3200 m located within a tropical oxygen minimum zone that caused deposition of laminated organic-rich sediments of latest Albian to earliest Campanian age. Upper Cenomanian to Lower Turonian sediments on Demerara Rise are mainly expressed by distinctly laminated black shales with well-preserved fish debris and phosphatic nodules. Within this black shale sequence light-colored, laminated foraminiferal packstones and wackestones occur (Shipboard Scientific Party, 2004). A detailed sedimentological description is given by Erbacher et al. (2004).

Linear sedimentation rates (LSRs) were estimated by the Shipboard Scientific Party (2004) from age-depth plots by fitting curves to available biostratigraphic and paleomagnetic data over certain depth intervals. Poor preservation or even absence of microfossils and the ambiguous interpretation of paleomagnetic data limit the bio- and magnetostratigraphic age assignment in most of the black shale sequences (Cenomanian–Santonian). Therefore, LSRs calculated for these intervals (0.3–0.5 cm/ka at Sites 1257, 1258, and 1259 and slightly higher values of ~0.85 cm/ka at Sites 1260 and 1261) should be considered as imprecise estimates.

Stable isotope stratigraphy provided by Erbacher et al. (2005) allows a detailed correlation of the investigated sites through the OAE 2 interval. At all studied sites, a distinctive positive carbon isotope excursion (~6.5‰) of the OAE 2 was identified (Fig. 2). The same authors

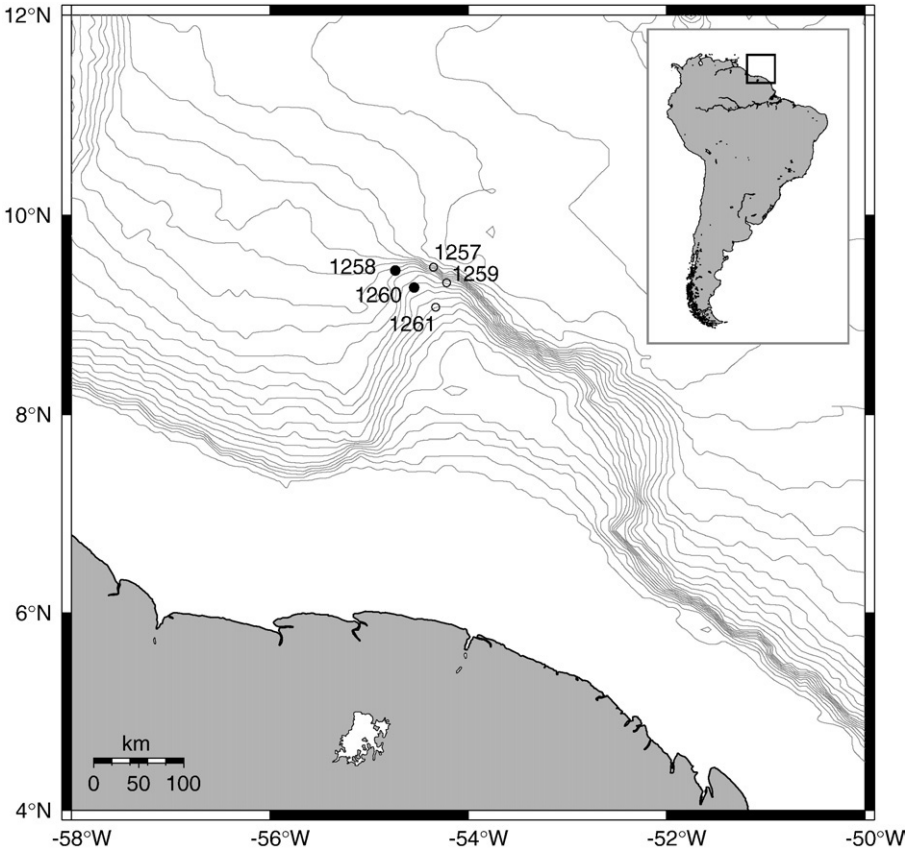

Fig. 1. Geographic position of Sites 1257–1261 at Demerara Rise (ODP Leg 207). (Online Map Creation www.aquarius.geomar.de).

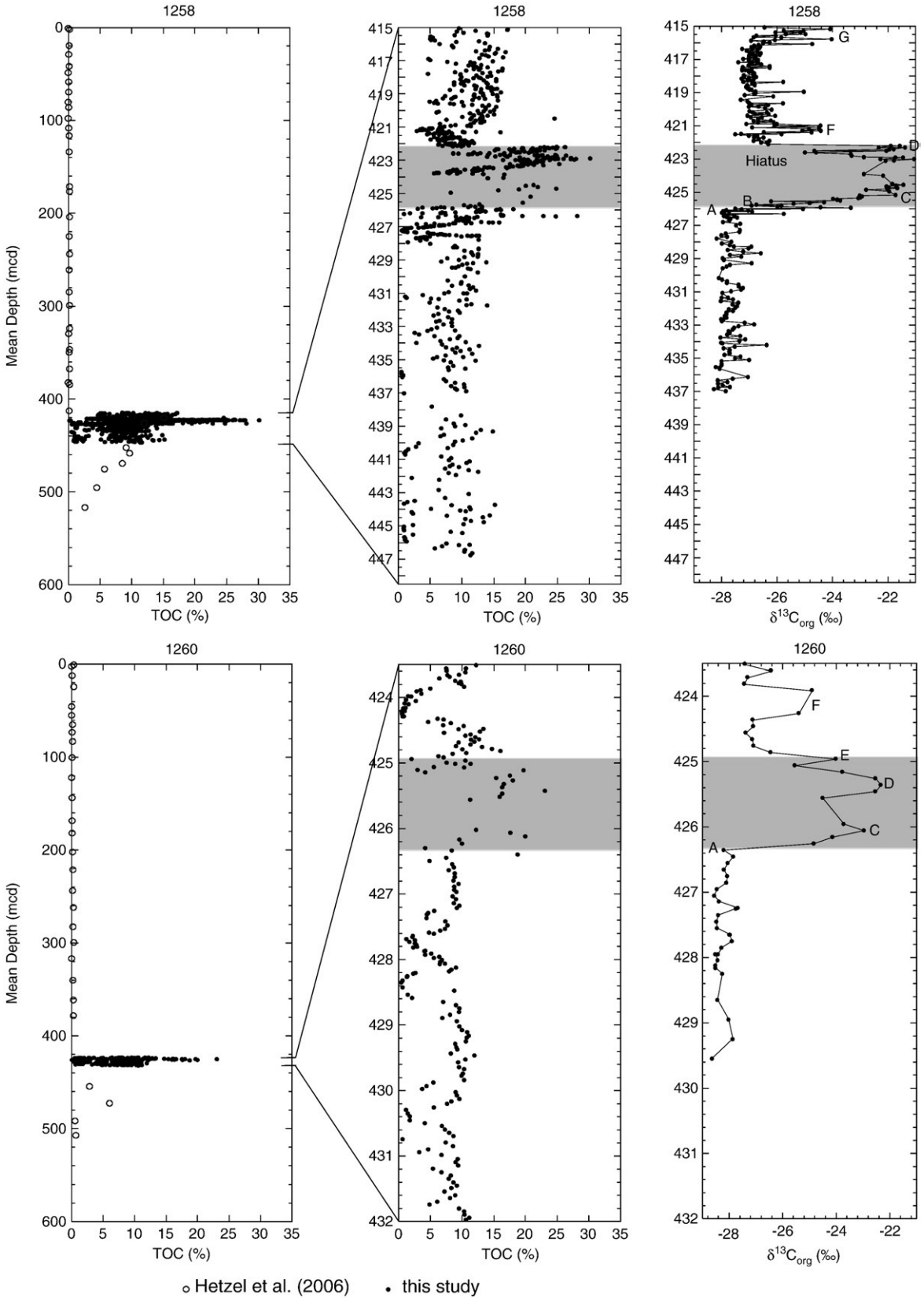

Fig. 2. Depth-profiles for TOC contents for the whole sediment column investigated (open circles) (Hetzel et al., 2006) and for Cenomanian/Turonian black shales at Demerara Rise, ODP Sites 1258 and 1260. Grey: OAE 2; $\delta^{13}C_{org}$-curve after Erbacher et al. (2005).

were able to correlate a number of short-termed $\delta^{13}C_{org}$ peaks and troughs within and above the excursion interval between the investigated sites. The events of this record include: (1) The onset of the excursion labeled "A". (2) A short-termed minimum "B" (not present at Site 1260). (3) An interval "C" with $\delta^{13}C_{org}$ values rising to −23 and −21‰. (4) The final maximum value "D". (5) A short positive peak "E" occurs during the general decrease in isotope values (not present at Site 1258). In addition, Erbacher et al. (2005) also correlated two peaks ("F"

and "G") located above the OAE 2 between the sites. Assuming a duration of ~400 ka for the interval between "A" (onset of excursion) and "D" (end of plateau) Erbacher et al. (2005) calculated average sedimentation rates between ~0.25 cm/ka (Site 1260) and ~1 cm/ka (Site 1258) for the OAE 2. There is no more detailed information available about sedimentation rates for the intervals above and below OAE 2 or variations within this interval.

In this study, two ODP sites along the Demerara Rise paleodepth-transect (Sites 1258 and 1260, see Table 1) were chosen to reconstruct paleoenvironmental changes during the late Cenomanian to earliest Turonian black shale deposition interval. Depths are expressed in meters composite depth (mcd), following the shipboard splice between the different holes drilled at each site (Shipboard Scientific Party, 2004).

2.1.1. ODP Site 1258

Site 1258 is located in a water-depth of 3192.2 m below modern sea level (mbsl) on the gently dipping western slope (~2°) of Demerara Rise. It is the deepest location in the SE–NW paleoceanographic depth transect across Demerara Rise (Shipboard Scientific Party, 2004). The 4 m-thick OAE 2, as defined by the pronounced $\delta^{13}C_{org}$ excursion, is located at a depth of 426–422 mcd (Erbacher et al., 2005). Based on $\delta^{13}C_{org}$ measurements, Erbacher et al. (2005) described a hiatus in the uppermost part of the OAE. The sediments of the investigated section comprise finely-laminated dark shales with occasional beds of phosphatic nodules, stringers of very dark homogeneous shales, and rare concretionary limestone nodules. Thirty-three and a half meters (415–448.5 mcd, see Table 2) of upper Cenomanian to lowermost Turonian laminated black shale sediments were investigated from a spliced interval of Holes 1258A, 1258B, and 1258C. 845 samples were taken at 1 cm resolution for the OAE 2 interval and at ~10 cm in underlying sediments. Assuming a sedimentation rate of ~1 cm/ka the studied interval covers a time span of ~3.35 Ma of deposition.

2.1.2. ODP Site 1260

Site 1260, in a water-depth of 2548.8 mbsl, is positioned on the gently dipping (~1°) northwest-facing slope of Demerara Rise, at an intermediate depth in the SE–NW paleoceanographic depth transect. The 1.4 m thick OAE 2 is located between 426.4 and 425.0 mcd, being thus much thinner than at Site 1258. Lithologically, the interval is very similar to Site 1258, although phosphatic nodules are not as common as at the deeper site (Erbacher et al., 2005). About 8.5 m of upper Cenomanian to lowermost Turonian laminated black shale sediments were sampled every ~5 cm (219 samples in total, see Table 2) from a spliced interval of Holes 1260A and 1260B. Sedimentation rates of the OAE 2 interval are estimated to be on the order of approximately 0.25 cm/ka, thus leading to the same duration of ~3.4 Ma of deposition for the studied sequence.

2.2. Analytical methods

Sediments splits were freeze-dried, ground and homogenized in an agate ball mill. For X-ray fluorescence (XRF) analysis (Philips® PW 2400 X-ray spectrometer), 600 mg of sample powder were mixed with 3600 mg of a 1:1 mixture of dilithiumtetraborate ($Li_2B_4O_7$) and lithium-metaborate ($LiBO_2$), or with 100% dilithiumtetraborate for carbonate-rich samples, preoxidized at 500 °C with NH_4NO_3 (p.a.) and fused to glass beads. Total sulfur (S_T) and total carbon (TC) were analyzed using an ELTRA® CS-500 IR-analyzer. Total inorganic carbon (TIC) was determined coulometrically by a UIC® CM 5012 CO_2 coulometer coupled to a CM 5130 acidification module. Total organic carbon (TOC) was calculated as the difference between TC and TIC. Procedures and accuracy of the methods were checked with in-house reference materials (Prakash Babu et al., 1999; see Appendix A). Different sedimentary sulfur fractions, chromium-reducible sulfur (S_P, essentially pyrite), organic matter (essentially kerogen-bound organic sulfur, S_{ORG}) and acid volatile sulfur (S_{AVS}) were separated quantitatively from powdered freeze-dried samples, as described by Böttcher et al. (2006). Chromium reducible sulfur, essentially pyrite sulfur, S_P, was extracted for 2 h via hot acidic Cr(II)Cl_2 (Zhabina and Volkov, 1978; Canfield et al., 1986; Fossing and Jørgensen, 1989). Liberated H_2S was precipitated quantitatively in Zn acetate traps and measured spectrophotometrically (Cline, 1969). The organic sulfur fraction, S_{ORG}, was calculated as the difference of total sulfur and the sum of chromium-reducible sulfur (Böttcher et al., 2006). S_{AVS} was extracted from selected samples from Site 1258 via anaerobic distillation with 6 M HCl (1 h). Since FeS is not expected in the black shale samples to survive the diagenetic pyritization and lab-based freeze-drying process, the S_{AVS} fraction is assumed to correspond to acid-volatile metal monosulfides. ZnS, for instance, that might have been formed in a euxinic water column, has been found in C/T samples in the present study via SEM-EDX, and has also been reported in Cretaceous black shales previously (Brumsack, 1980). ZnS would have survived burial and later sample handling.

The amount of pyrite iron (Fe_P) was calculated from the S_P content assuming ideal stoichiometry. This fraction essentially represents the total highly reactive iron fraction (Raiswell and Canfield, 1998; Poulton and Raiswell, 2002). To confirm this approach, iron-oxide bound iron was separately determined in selected black shale samples from Sites 1258 and 1260 and presented by Böttcher et al. (2006). As described in detail by these authors, iron(oxyhydr)oxide phases were extracted from sediment samples using a buffered solution of Na dithionite and extracted iron was determined spectrophotometrically. It was found that this fraction is only present in very small amounts and that pyrite iron amounts to 96–99% of the total highly reactive iron pool. For samples from Site 1258 $^{34}S/^{32}S$ ratios of the S_P bound sulfur were determined by means of C-irmMS using a Eurovector 3000 elemental analyzer (EA) coupled to a Thermo Finnigan MAT253 and are given in the δ-notation versus the international V-CDT standard. Calibration of the mass spectrometer was carried using international IAEA and NBS reference materials. Sulfur isotope results for Site 1260 will be presented in a separate communication (Böttcher et al., in prep.).

Finally, selected non-ground carbon-coated (BAL-TEC sputter-coating device SCD 005) freeze-dried sediment samples were investigated by means of energy-dispersive X-ray analysis on an Oxford Link ISIS 300 EDX-System with Pentafet S ATW Si-detector installed on a Zeiss DSM 940 scanning electron microscope (SEM).

Table 1
Drilling locations Site 1258 and 1260, ODP Leg 207

Site	Hole	Latitude	Longitude	Water depth (mbsl)	OAE 2 interval (mcd)	SR (cm/ka)
1258	A	9° 26.000′N	54° 43.999′W	3192.2	425.95–422.18	~1
1258	B	9° 26.000′N	54° 43.982′W	3192.2		
1258	C	9° 26.000′N	54° 43.966′W	3192.2		
1260	A	9° 15.984′N	54° 32.633′W	2548.8	426.34–424.94	~0.25
1260	B	9° 15.931′N	54° 32.652′W	2548.8		

mbsl = meters below sea level; mcd = meters composite depth; SR = sedimentation rate.

Table 2
Sampling Site 1258 and 1260

Site	Sampled interval (mcd)	Number of samples	Time of deposition (Ma)	Sampling resolution (cm)	Sampling resolution (ka)
1258	415.0–448.5	845	~3.35	~1/~10	~1/~10
1260	423.5–432.0	219	~3.40	~5	~20

mcd = meters composite depth.

3. Results and discussion

3.1. Preliminary remarks

To account for dilution effects by varying carbonate or organic matter contents trace element contents were normalized to Al (TE/Al ratio). In cases of very low Al contents (see Figs. 3 and 4), normalization may lead to exaggerated peaks in TE/Al ratios, which has to be kept in mind when interpreting TE/Al profiles (van der Weijden, 2002). Some elements, like Al, Ti, K, Rb and Zr, are only present in the detrital component and are not

influenced either by biogenic or diagenetic processes. Significant variations in TE/Al ratios of these elements therefore reveal changes in source area composition. While most of the investigated sediment intervals show TE/Al ratios similar to average shale (AS; Wedepohl, 1971, 1991), several sediment layers of one centimeter to several decimeters thickness were identified by characteristic TE/Al ratios. At Site 1260 a 35 cm thick interval (425.61–425.96 mcd) within the OAE 2 is characterized by low K/Al (0.07, AS=0.34), high Ti/Al ratios (0.102, AS=0.053) and is depleted in Si (Si/Al 2.58, AS=3.11; see Appendix B). From macroscopic observation (Appendix B-b), this interval most likely is a diagenetically altered ash bed. At Site 1258, three sediment layers within OAE 2 (423.51–423.53 mcd, 423.87–424.04 mcd, and 425.22–425.50 mcd) correspond to this layer, identified by similar disturbances in TE/Al profiles. At both sites abrupt changes in carbonate, TOC and TS contents from extremely high concentrations to near zero values can be identified. Light $\delta^{13}C$ values of the carbonate in the discussed interval at Site 1260 (Friedrich, pers. communication) point towards the involvement of microbiological processes like anaerobic oxidation of methane (AOM) (e.g., Galimov, 2006). The production of bicarbonate by AOM could result in the precipitation of authigenic carbonates, and thus increase the degree of carbonate diagenesis implying recrystalization of carbonates from foraminifera and nanofossils (Erbacher et al., 2004). With the geochemical methods applied (bulk element concentrations) the origin of the material can not be identified. To avoid misinterpretation of changes in element distribution patterns, samples from these intervals (7 samples from Site 1260 and 27 samples from Site 1258) were excluded from following discussion regarding changes of redox-conditions and trace metal availability. As the bulk geochemistry of sites is similar, analytical results of discussed intervals are given as average values listed in Appendix B-c.

3.2. Bulk parameters

Fig. 2 shows the depth profiles of total organic carbon (TOC) for the whole sediment column (data from Hetzel et al., 2006) and the upper Cenomanian to lower Turonian black shale sequences (C/T back shales), which are in the focus of this study.

Sediments above these sequences are characterized by low TOC contents (<0.4%). Below these intervals TOC contents decrease from ~10% to ~1% with increasing depth. The C/T black shales show varying TOC values: lowest contents (almost 0%) in carbonate-rich layers and highest contents (30.2% at Site 1258 and 23.1% at Site 1260) within the OAE 2 interval, which is identified by correlation with the $\delta^{13}C_{org}$ curve from Erbacher et al. (2005) and marked in grey.

Figs. 3 and 4 show the bulk chemistry of the C/T black shales: as mentioned above, highly variable TIC contents (<0.2–11.8%) lead to dilution effects, which are shown by the inverse distribution pattern for TIC and Al, representing terrigenous detritus. The TIC profiles display the light–dark cycles described by the Shipboard Scientific Party. Whereas the profile of Site 1260 suggests a regular cyclicity possible modulated by orbital forcing, carbonate contents of Site 1258 show a less regular distribution pattern despite higher resolution (see Table 2). For both sites, time series analysis of our high-resolution TIC data does not evidence orbital cyclicity.

Nederbragt et al. (2007) analyzed the cyclicity during the Mid-Cretaceous at Demerara Rise. Due to the irregular spacing of the carbonate-rich and organic-rich cycles (lack of precise age control, variable sedimentation rates and/or degree of compaction and minor hiatuses), the authors concluded instead of establishing a continuous cyclostratigraphy for the entire organic-rich unit to perform time series analysis of sediment color data in selected intervals in combination with thin section analysis of representative lithologies. They found that cyclic variation in lithology at Demerara Rise is inferred to represent eccentricity and precession cycles with a weak obliquity component. For analysis of the cyclicity during OAE 2 the authors examined two cores from Site 1258 and 1260. Both, precession and eccentricity cycles were found.

To better compare TOC and S_T contents for Demerara C/T black shales with other C/T sections we calculated TOC_{cf} and $S_{T\,cf}$ for a carbonate-free sediment. Profiles are given in Figs. 3 and 4 beside profiles of absolute concentrations. For Site 1258 most of the TOC values vary between ~0.5 and ~15%. Adjusting for dilution by carbonate resulting TOC_{cf} values are quite higher (~10–~25%). Some intervals of half a meter thickness are characterized by TOC contents >20%. These peaks are distributed right below, within and above OAE 2. For Site 1260 the TOC contents vary between ~0.5 and ~12% and on a carbonate free basis TOC_{cf} values fall between ~15 and ~22%. Highest TOC contents (>15%) are found within OAE 2.

Average contents below, within and above OAE 2 (Table 3) show higher TOC and lower TIC contents for Site 1258 in comparison to Site 1260. For both sites, average TOC values are in the same range (TOC: 6.9–10.1%; TOC_{cf}: 17.6–19.3%) below and above the OAE 2 and slightly higher during the OAE 2 with 17.8% (TOC_{cf} 22.4%) at Site 1258 and 12.1% (TOC_{cf} 22.8%) at Site 1260. The same is true for S_T values with 1.5–2.4% ($S_{T\,cf}$ 3.8–4.7%) below and above and 5.0% ($S_{T\,cf}$ 6.3%) within the OAE 2 at Site 1258 and 3.4% ($S_{T\,cf}$ 6.5%) within the OAE 2 at Site 1260.

3.3. Iron

Figs. 3 and 4 show profiles of total iron and Al-normalized iron contents. Only for some carbonate-rich layers Fe contents are below the quantification limit of 0.33% (e.g. ~424 mcd at Site 1260) and Fe_T/Al peaks may be exaggerated (see Section 3.1.) due to inaccuracies of measurements of Fe and Al close to or below the quantification limit. Besides these peaks, the Fe_T/Al profiles show an almost constant value close to AS. Assuming severe oxygen-deficiency, as evidenced by sediment lamination for the black shale sequence of Demerara Rise, the almost constant average shale-like values of Fe_T/Al imply anoxic but not euxinic (no free H_2S in the water column) conditions during deposition. Fe_T/Al ratio of the sediment is neither decreased via mobilization of iron(hydr)oxides under suboxic conditions nor increased via precipitation of dissolved Fe species as sulfide in the overlying water column under euxinic conditions. During OAE 2 Fe_T/Al mean values increase to 0.76 (Site 1258, maximum 1.72) and 0.80 (Site 1260, maximum 1.89), owing to an increase in total Fe_T contents. This indicates an additional Fe-source during deposition of this interval. In analogy to the modern Black Sea reductive Fe mobilization in near-shore areas or enhanced fluvial input are likely causes for the observed Fe-enrichment (e.g., Lyons and Severmann, 2006). In the case of the modern Black Sea Fe_T/Al-ratios are increasing with water depth (e.g. Wijsman et al., 2001) because syngenetic iron sulfides form an increasing part of bulk sedimentary iron. This model requires truly euxinic conditions, besides the existence of a zone where reducing but non-sulfidic conditions prevail, allowing Fe transport from shallow to deep sites (e.g., Lyons and Severmann, 2006). The increase of the ratio of pyrite iron to total iron, Fe_P/Fe_T, from a mean value of 0.44 below and above to about 0.64 (Table 4) within OAE 2 indicates the addition of syngenetic water column-derived pyrite (Raiswell and Canfield, 1998; Poulton and Raiswell, 2002; Böttcher et al., 2006, and references therein). Together with previous measurements on the detailed reactive iron speciation of Leg 207 sediments (Böttcher et al., 2006), these findings are confirmed by the Al-normalized iron contents, as discussed above. Fig. 5 presents the analytical data of Sites 1258 and 1260 in a ternary Fe_x–S_T–TOC plot (Brumsack, 1988; Dean and Arthur, 1989; Brumsack et al., 1995). The represented data within the OAE all plot below the pyrite-saturation line indicating, that under iron-limited conditions, some (excess) sulfide and/or sulfur intermediates were able to react with organic matter to form organic sulfur compounds.

3.4. Sulfur and sulfur isotopes

Dissimilatory sulfate reduction leads to the formation of hydrogen sulfide that may transform reactive iron to iron sulfides (essentially

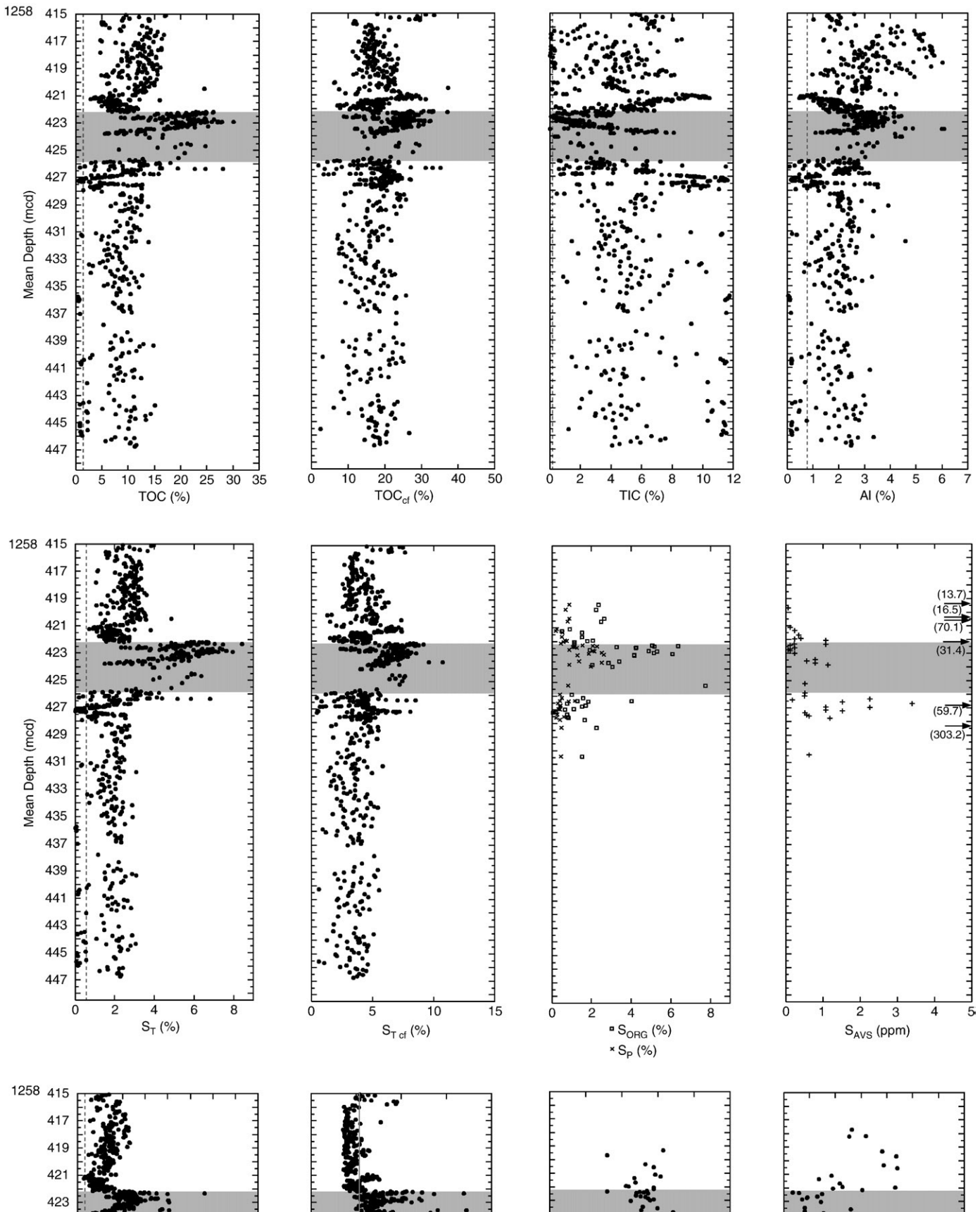

Fig. 3. Depth-profiles for TOC, TIC, Al, S_T, S_{ORG}, S_P, S_{AVS} and Fe_T for Cenomanian/Turonian black shales at Site 1258. TOC_{cf} and $S_{T\,cf}$ are calculated for carbonate-free sediment. $\delta^{34}S$ of pyrite, Fe_T/Al ratios as well as Fe_P/Fe_T ratios are also shown. Grey: OAE 2; grey solid line: element/Al ratio of to 'average shale' (AS) (Wedepohl, 1971, 1991); dashed line: quantification limit (see Appendix A).

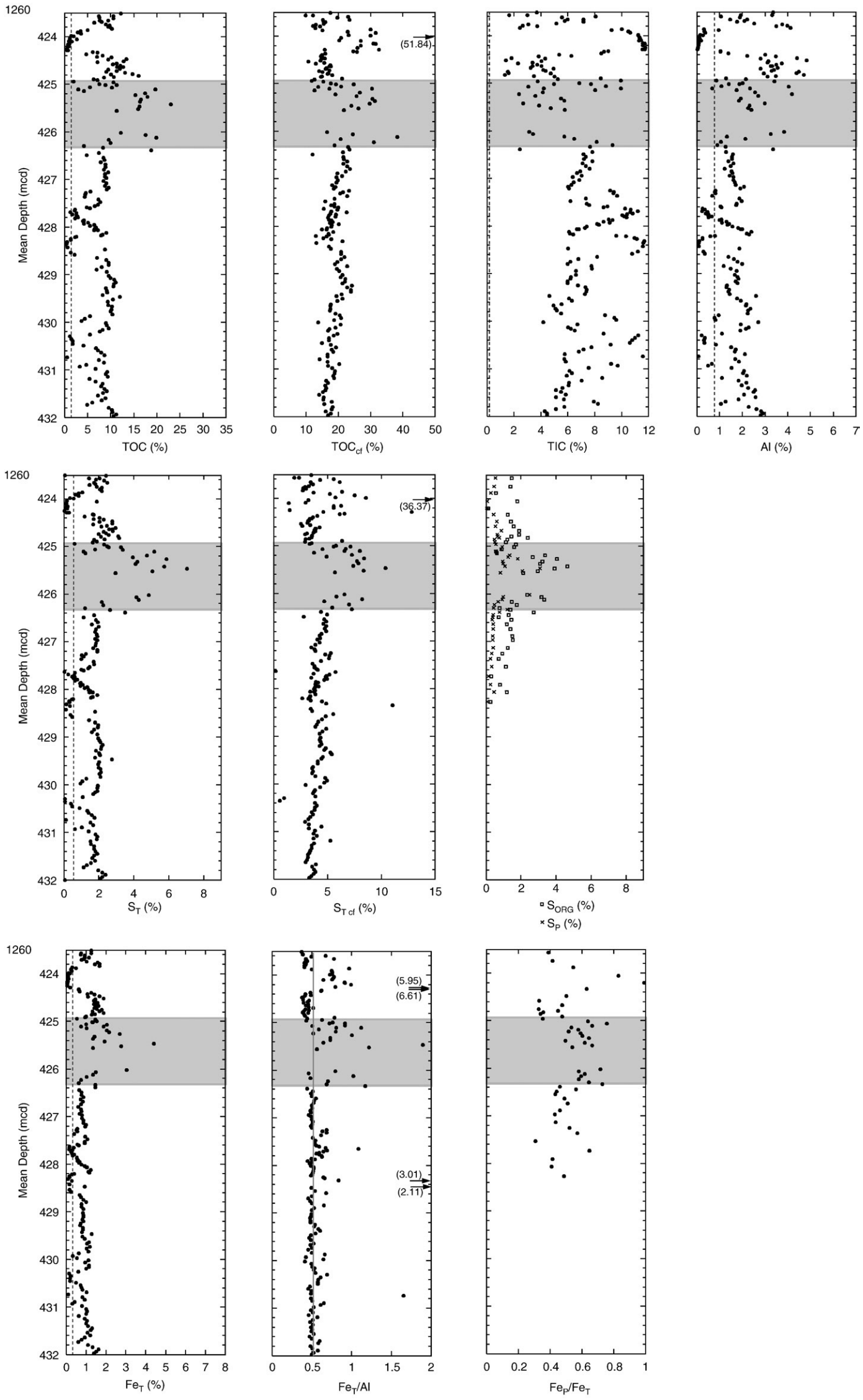

Fig. 4. Depth-profiles for TOC, TIC, Al, S_T, S_{ORG}, S_P and Fe_T for Cenomanian/Turonian black shales at Site 1260. TOC_{cf} and $S_{T\,cf}$ are calculated for carbonate-free sediment. Fe_T/Al ratios as well as Fe_P/Fe_T ratios are also shown. Grey: OAE 2; grey solid line: element/Al ratio of 'average shale' (AS) (Wedepohl, 1971, 1991); dashed line: quantification limit (see Appendix A).

Table 3
Comparison of average element contents and element/Al ratios Cenomanian/Turonian black shales of Demerara Rise and 'average shale'

		1258 below OAE 2 (n=347)	1258 within OAE 2 (n=197)	1258 above OAE 2 (n=274)	1260 below OAE 2 (n=129)	1260 within OAE 2 (n=26)	1260 above OAE 2 (n=57)	Average shale (Wedepohl, 1971, 1991)
S_T	%	1.71	4.97	2.35	1.45	3.43	1.69	0.24
TIC	%	6.20	2.46	5.00	7.59	5.76	6.34	0.35
TOC	%	7.83	17.82	10.13	6.89	12.12	7.54	
Si	%	11.61	14.66	11.43	6.64	8.06	9.14	27.53
Ti	%	0.08	0.14	0.12	0.08	0.10	0.10	0.46
Al	%	1.68	2.90	2.57	1.47	2.17	2.18	8.84
Fe_T	%	0.88	2.17	1.19	0.76	1.65	0.97	4.80
Mg	%	0.47	0.46	0.57	0.47	0.47	0.60	1.60
Ca	%	21.37	9.44	18.27	26.04	20.20	22.32	1.57
Na	%	0.68	1.16	0.99	0.74	0.86	0.82	1.19
K	%	0.45	0.89	0.74	0.43	0.65	0.69	2.99
P	%	0.25	0.15	0.54	0.29	0.22	0.52	0.07
As	ppm	13	25	21	18	25	16	10
Ba	ppm	260	542	612	343	746	642	580
Co	ppm	*3*	13	*5*	*3*	9	*4*	19
Cr	ppm	121	70	149	109	82	145	90
Cu	ppm	58	68	70	53	68	63	45
Mn	ppm	*7*	*50*	*27*	*0*	*14*	*7*	850
Mo	ppm	80	40	95	62	33	38	1
Ni	ppm	126	169	149	108	144	92	68
Rb	ppm	21	30	30	19	22	26	140
Sr	ppm	593	653	716	923	952	792	300
U	ppm	12	17	18	16	18	12	4
V	ppm	1058	370	1173	1386	554	899	130
Y	ppm	12	29	23	13	23	19	41
Zn	ppm	578	138	968	879	382	701	95
Zr	ppm	28	38	36	27	33	34	160
$S_{T\ cf}$	%	3.83	6.26	4.36	4.04	6.47	4.70	0.25
TOC_{cf}	%	17.64	22.40	18.30	18.74	22.80	19.30	
S_T/Al		1.05	1.75	1.05	1.06	1.67	1.54	0.03
TOC/Al		4.85	6.32	4.40	4.94	5.93	5.98	
Si/Al		7.79	5.81	4.76	4.49	3.72	4.24	3.11
Ti/Al		0.05	0.05	0.05	0.05	0.05	0.05	0.05
Fe_T/Al		0.55	0.76	0.50	0.58	0.80	0.74	0.54
Mg/Al		0.57	0.17	0.25	0.55	0.25	1.39	0.18
Ca/Al		42.97	4.36	11.69	43.01	13.87	121.32	0.18
Na/Al		0.43	0.41	0.42	0.57	0.42	0.58	0.13
K/Al		0.28	0.31	0.29	0.32	0.31	0.40	0.34
P/Al		0.13	0.05	0.20	0.17	0.12	0.23	0.01
As/Al	$\times 10^{-4}$	9.3	8.8	8.4	14.3	12.5	13.6	1.1
Ba/Al	$\times 10^{-4}$	190.8	188.1	239.0	271.8	345.2	531.6	65.6
Co/Al	$\times 10^{-4}$	2.1	4.4	2.3	2.2	4.4	3.2	2.1
Cr/Al	$\times 10^{-4}$	68.8	24.0	50.7	75.1	37.5	57.7	10.2
Cu/Al	$\times 10^{-4}$	36.0	24.0	27.4	38.9	30.5	45.9	5.1
Mn/Al	$\times 10^{-4}$	9.2	18.4	23.2	0.1	5.9	36.2	96.2
Mo/Al	$\times 10^{-4}$	50.0	14.3	40.4	49.4	16.7	20.3	0.1
Ni/Al	$\times 10^{-4}$	77.8	59.5	62.0	85.0	73.0	47.6	7.7
Rb/Al	$\times 10^{-4}$	11.5	10.2	11.3	12.1	10.7	10.6	15.8
Sr/Al	$\times 10^{-4}$	584.4	241.5	349.0	1019.4	541.5	1425.7	33.9
U/Al	$\times 10^{-4}$	9.7	6.2	8.5	14.5	10.8	17.9	0.4
V/Al	$\times 10^{-4}$	654.8	127.0	461.7	1010.1	294.5	439.8	14.7
Y/Al	$\times 10^{-4}$	8.9	10.1	10.2	10.6	13.1	17.0	4.6
Zn/Al	$\times 10^{-4}$	316.0	48.1	355.9	581.4	154.0	251.1	10.7
Zr/Al	$\times 10^{-4}$	20.7	13.5	14.9	22.4	17.1	31.8	18.1

Italics: average values below quantification limit (see Appendix A).

pyrite, FeS_2; including framboidal pyrite Fig. 6) and, under iron limited conditions with organic matter to form organic sulfur compounds (e.g. Werne et al., 2004). The profiles of S_P and S_{ORG} show elevated values during OAE 2 at both sites (Figs. 3 and 4; see also Table 4). Below OAE 2 S_P values are ~0.4% (ca. 25 rel% of S_T) and S_{ORG} ~1.2% (respectively ca. 75 rel% of S_T). At Site 1258, S_P contents rise to ~1.7% (maximum >2.5%) and S_{ORG} to ~4.4% (maximum >7.7%) within the OAE 2 interval, thus the proportion of pyrite sulfur increases to ca. 28 rel% of total sulfur. Although absolute values are not as high as at Site 1258, the pyrite sulfur fraction at Site 1260 reaches even ca. 33 rel% with 1.1% S_P (maximum >3.1%) and 2.3% S_{ORG} (maximum >6.6%) during OAE 2. Above OAE 2 the proportional composition of different sulfur species nearly equals the composition below with ~0.5% S_P and ~1.4% S_{ORG} (S_P:S_{ORG}=26:74 rel%) at both sites. The relationship of S_P with TOC data is presented in Fig. 7a and compared to the relationship proposed for "normal marine sediments" (Berner and Raiswell, 1983). Only a few data points coincide with the relation found for clastic sediments below an oxic water column (dashed line in Fig. 7a). A number of data points plot above the regression line, indicating an

Table 4
Average pyrite sulfur (S_P), pyrite iron (Fe_P), acid volatile sulphur (S_{AVS}), calculated organic sulfur (S_{org}) and ratio of pyrite (reactive) iron to total iron (see Table 3)

		1258 below OAE 2 (n=19)	1258 within OAE 2 (n=18)	1258 above OAE 2 (n=12)	1260 below OAE 2 (n=16)	1260 within OAE 2 (n=22)	1260 above OAE 2 (n=13)
S_P	%	0.42	1.68	0.60	0.38	1.14	0.52
Fe_P	%	0.36	1.46	0.52	0.33	0.99	0.45
S_{AVS}	ppm	22.4 (n=17)	0.5 (n=13)	12.2 (n=11)			
S_{org}	%	1.25	4.39	1.69	1.14	2.31	1.41
Fe_P/Fe_T		0.41	0.67	0.44	0.43	0.60	0.46

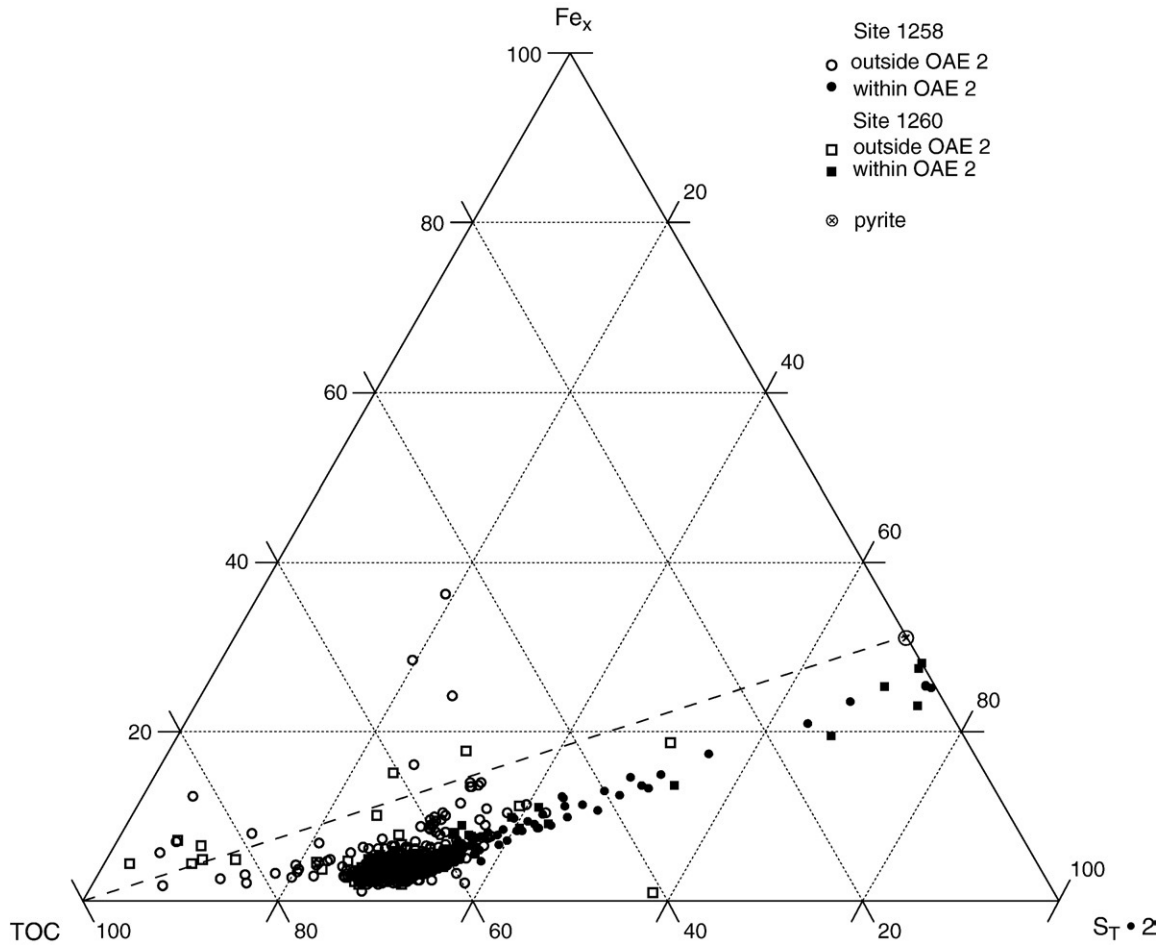

Fig. 5. Ternary plot: degree of pyritization of Cenomanian/Turonian black shales at Demerara Rise in the Fe_x–TOC–$S_T \cdot 2$ system (relative weight ratios). Reactive Fe_x is calculated with $Fe_x = Fe_T - 0.25 \cdot Al$. Data point for pyrite is also shown.

excess of sulfur that may be due to euxinic depositional conditions. At highest TOC contents, however, most data show a relative excess of organic matter (OM). The indicated iron-limitation during black shale deposition has also been found for the modern Black Sea sapropel and Mediterranean sapropels (e.g. Lyons and Berner, 1992; Passier et al., 1999b; Böttcher et al., 2006). S_P in the investigated black shale samples makes up between 30% and 100% of S_T, with a decrease of the relative amount of S_P with increasing OM content. This indicates the importance of the balance between organic matter and the syngenetic metal flux to the surface sediments in controlling the sedimentary sulfur speciation. In addition to fixation of sulfide by the reaction with iron, organic matter acted as the second important sulfur trap during early diagenesis. From molecular analysis of the preservation pathways of sedimentary organic carbon in a euxinic environment Hebting et al. (2006) proposed that sulfides produced by bacterial sulfate reduction play a major role for the reductive alteration and thus preservation of organic carbon. From the nearly linear variation of organic sulfur and organic carbon contents (Fig. 7b), essentially constant atomic S_{ORG}/TOC ratios are obtained. Quantitatively, the samples with TOC contents exceeding ~2 wt.% have as much as 10 atom% organic sulfur. Most of the atomic S/C ratios fall in the range of 0.04 to 0.06, which is within the range reported for sapropels from the Mediterranean and Black Sea (Passier et al., 1999b; Böttcher et al., 2006). The almost linear relationship between TOC and S_{ORG} may be caused by a constant relative proportion of organic matter fractions available for diagenetic sulfurization.

The downcore variation of the stable sulfur isotope composition of pyrite at Site 1258 displays a range in $\delta^{34}S$ values between −28.2 and +0.2‰ (average −15.4±8.3‰; n=41) during OAE 2, with an inverse relationship to the $\delta^{13}C$ values (Fig. 3, Table 5). The sulfur isotope variations observed in the sedimentary pyrite pool are much more pronounced than those observed in the global seawater sulfate at this time (Paytan et al., 2004). This indicates that sulfur isotope discrimination was controlled by changes in sedimentary conditions and was higher during times of enhanced burial of OM. This can be caused by a lower burial efficiency of reduced sulfur and/or higher contributions from the oxidative part of the sulfur cycle (in the water column or in surface sediments). A similar trend and magnitude of sulfur isotope discrimination was found in the C/T sediments of different sites in the Tarfaya basin (e.g. Kolonic et al., 2002; Böttcher et al., unpublished data). For instance for the pyrite fraction Böttcher et al. (unpublished data) obtained ranges at Site S13 (−18.9 to +2.5‰, average −10.2±7.8‰; n=9), at S57 (−28.8 to −8.8‰, average −17.6±5.1‰; n=29), and S75 (−20.6 to −8.7‰, average −15.7±3.2‰; n=17). This similarity suggests a common control of the overall sedimentary sulfur isotope signal for the CTBE in the southern North Atlantic independent of paleo-water depths. The stratigraphic trend of the sulfur isotope ratios shows that pyrite isotope data go through a minimum similar to previous observations at Tarfaya (Kolonic et al., 2002; Böttcher et al., unpublished data). We relate the most negative values to an increased contribution of syngenetic pyrite, sulfur derived from the oxidative part of the biogeochemical sulfur cycle, and mostly changes in other factors (e.g., the quality of organic matter) influencing overall sulfur isotope discrimination. Most lighter sulfur isotope data are found during OAE 2 compared to sediments outside OAE 2 (Fig. 8), and these are associated with highest contents of pyrite-iron. This is in agreement with findings of Gauthier (1987) on Cretaceous black shales from the Western Interior Seaway. Taking the sulfur isotopic composition for seawater sulfate during the Cenomanian/Turonian to be around +15‰ (Strauss, 1999; Paytan et al., 2004), and assuming that

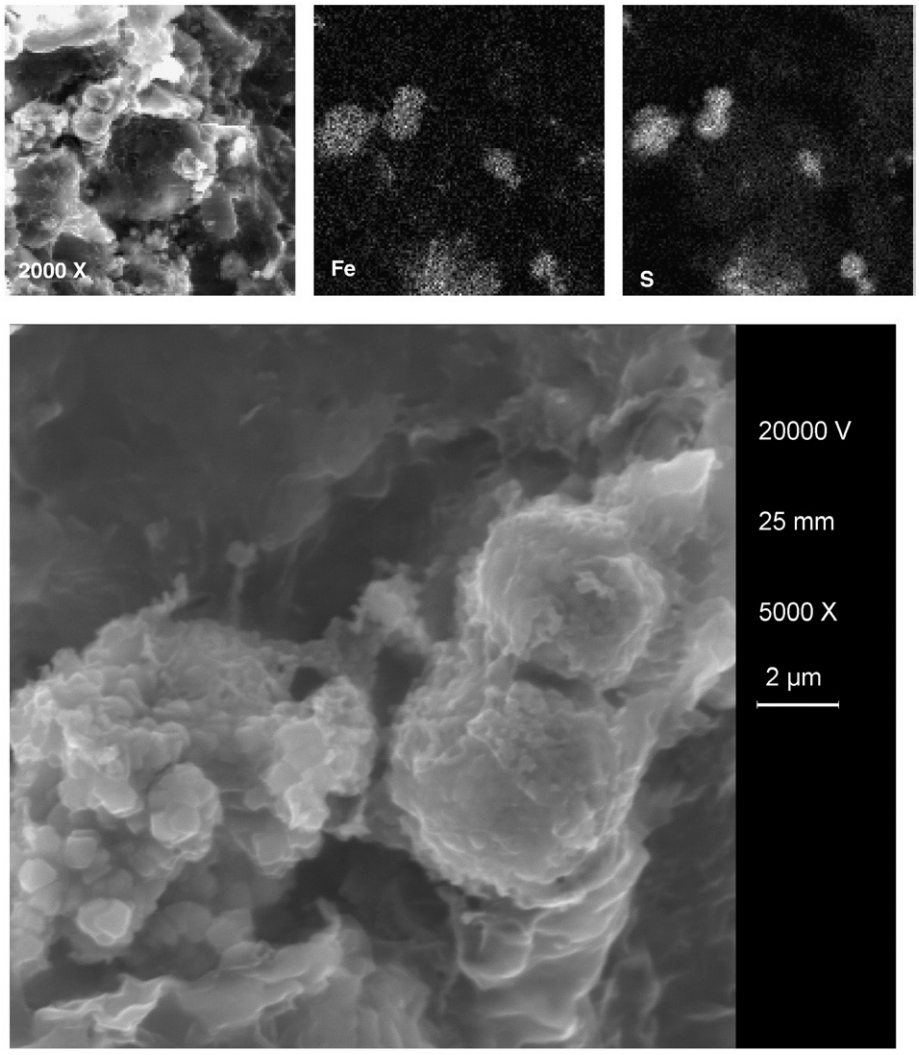

Fig. 6. EDX-Scan and SEM of a pyrite framboid from Site 1258B-45-4 138–139 cm, 422.98 mcd (within OAE 2).

pyrite mainly formed under conditions that were open with respect to dissolved sulfate (Hartmann and Nielsen, 1969), e.g., in the water column or close to the sediment–water interface, an overall sulfur isotope fractionation of 15 to 42‰ is estimated for Site 1258. This is within the range found in studies with pure cultures of sulfate-reducing bacteria (e.g. Brunner and Bernasconi, 2005), but is smaller than values found in C/T sediments from the northern North Atlantic (Böttcher and Kuypers, unpublished data), in the Pliocene TOC-rich sapropels of the deep Mediterranean (Passier et al., 1999a; Böttcher et al., 2003), in the modern euxinic Black Sea (Neretin et al., 2004; Böttcher et al., 2004), and in sediments from the Great Australian Bight (Wortmann et al., 2001). Higher contributions from the oxidative part of the sulfur cycle (microbial disproportionation of sulfur intermediates) and/or lower cellular sulfate reduction rates or specific bacterial communities may be responsible for the development of the different characteristic sulfur isotope signals.

3.5. Redox-sensitive and sulfide forming trace metals

3.5.1. Manganese

The C/T black shales of Demerara Rise are characterized by very low Mn-concentrations (Fig. 9). For most of the samples the Mn contents are below the XRF quantification limit of 78 ppm. At Site 1258, for sediments below 427.7 mcd Mn values are below the detection limit, which is defined as half the quantification limit. Right below, within and above OAE 2, Mn contents are higher and reach the detection limit of 39 ppm. Within OAE 2, Mn values show a high variability between detection limit and 426 ppm, with a mean value of ~50 ppm and a standard deviation of the same order (49 ppm). Above OAE 2 (421.63–421.03 mcd) a clear peak in absolute Mn concentrations with a maximum value of 217 ppm can be recognized. This peak can be correlated to a peak in TIC. Since Mn concentrations often are below the quantification limit, Mn/Al ratios have to be considered with caution. A maximum Mn/Al ratio of 466×10^{-4} at 421.63–421.03 mcd represents a significant Mn enrichment in comparison to the Mn/Al ratio of 96×10^{-4} for average shale (Wedepohl, 1971, 1991). The same is true for certain intervals within OAE 2. For samples close to the onset and termination of OAE 2, the enrichments in Mn are less pronounced.

At Site 1260 Mn concentrations in all samples are below the quantification limit. Only a few samples attain the detection limit of 39 ppm: One interval above OAE 2 (423.99–424.04 mcd) reaching Mn values up to 77 ppm can again be correlated to a carbonate peak. Within OAE 2 Mn concentrations vary between 0 and 46 ppm.

Extremely low Mn/Al ratios in C/T black shales of Demerara Rise indicate that Mn was either reduced within the water column before sedimentation or upon early diagenesis in an environment open to dissolved Mn(II) loss as provided by an expanded oxygen-minimum-zone (OMZ), like the modern upwelling zones off Peru (Böning et al., 2004) or in the Gulf of California (Brumsack, 1989). Thurow et al. (1992) found a similar mobilization of Mn at the Northwest Australian margin during OAE 2. The authors described Mn-poor sediments within the OMZ and Mn-rich sediments below the OMZ, indicating oxic deep waters during the C/T interval at this location.

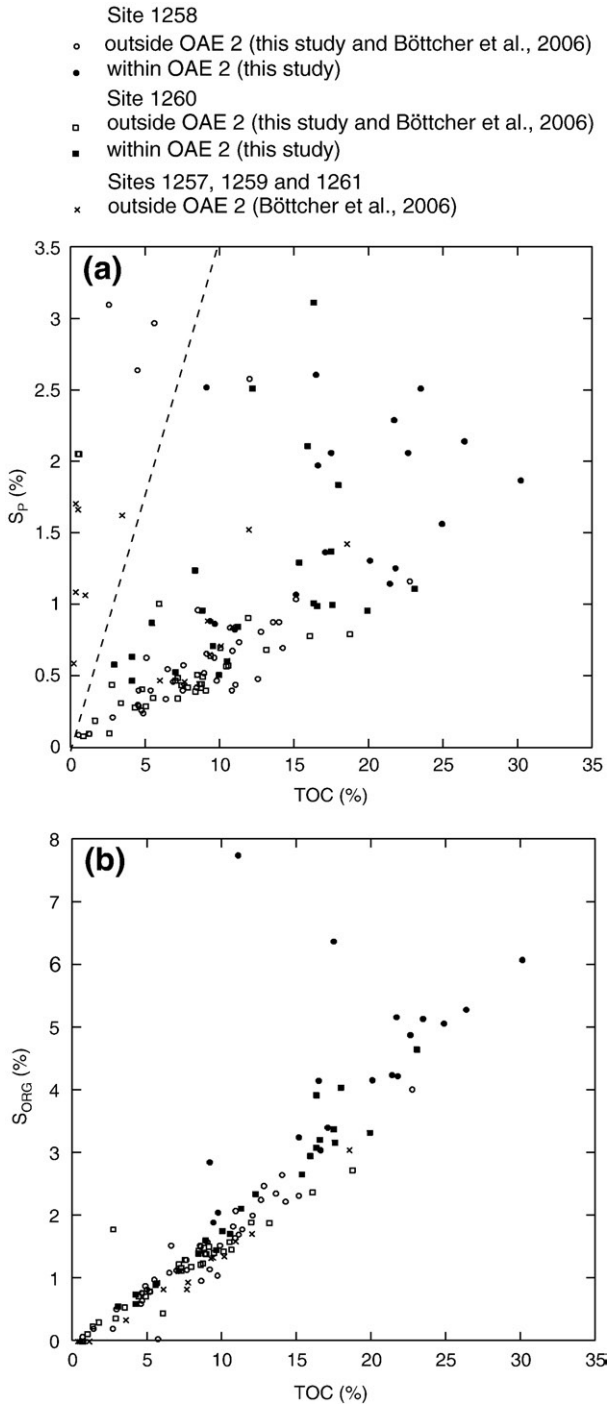

Fig. 7. (a) Pyrite sulfur (S_P) versus TOC and (b) organic sulfur (S_{ORG}) versus TOC for Cenomanian/Turonian black shales at Site 1258 and Site 1260 (this study) and black shale samples from Sites 1257, 1259 and 1261 (Böttcher et al., 2006). Dashed line marks the relationship derived for normal marine sediments as defined by Berner and Raiswell (1983).

A possibility for the observed Mn-enrichment might be the fixation of dissolved Mn(II) as mixed Mn–Ca-carbonates under conditions where Mn was enriched. Brumsack (2006) suggests that overgrowths of early diagenetic Mn-carbonate on pre-existing carbonate tests might be responsible for Mn enrichment in Black Sea sediments. Pre-existing carbonates may act as an efficient trap for diagenetically mobilized Mn(II) (Boyle, 1983; Gingele and Kasten, 1994; Böttcher, 1997).

Table 5
Average $\delta^{34}S$ of pyrite sulfur (S_P) for Cenomanian/Turonian black shales of Site 1258

		1258 below OAE 2 (n=16)	1258 within OAE 2 (n=12)	1258 above OAE 2 (n=13)
$\delta^{34}S_P$	‰	−8.4	−24.4	−15.6

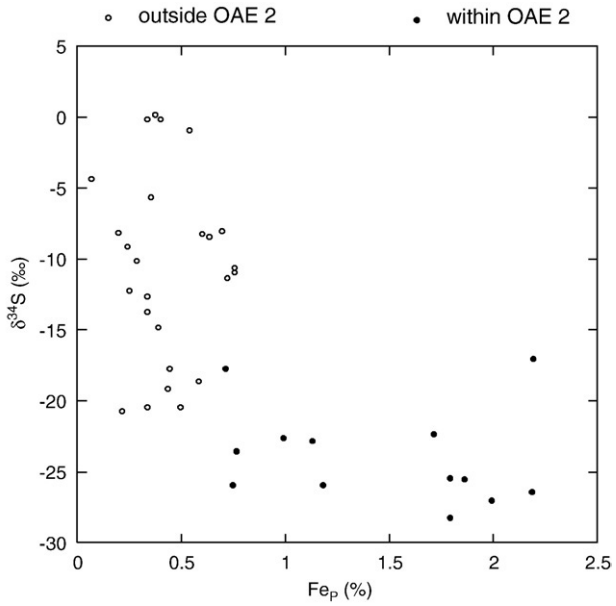

Fig. 8. $\delta^{34}S$ of pyrite versus pyrite iron (Fe_P) for Cenomanian/Turonian black shales at Site 1258.

At Demerara Rise elevated Mn/Al ratios are only seen in distinct horizons with high carbonate contents below (Site 1258) and above OAE 2 (Site 1258 and Site 1260). We therefore relate these Mn/Al peaks in C/T black shales to carbonate diagenesis. There is no correlation to Fe_T/Al ratios that would point to simultaneous mobilization from suboxic sediments and precipitation under sulfidic conditions as described by Lyons and Severmann (2006).

The higher Mn contents at Site 1258 might originate from the position in greater paleo-water depths. Assuming the existence of an OMZ, Site 1258 might be located below the OMZ where during times of weaker anoxia, Mn(IV)-bearing phases reached the sediment and later were transformed into mixed Ca–Mn-carbonates.

Within OAE 2, Mn values show a high variability as described above. As all OAE 2 samples with higher Mn/Al ratios are located near the presumed “ash-layers”, the import of Mn(IV)-bearing phases could also be attributed to the different detritus composition (average Mn contents: 332 ppm compared to 17 ppm mean value for all C/T black shales of this study, see Appendix B-c). If Mn was released to the pore space after burial, Mn concentrations in the pore water within these “ash-layers” and adjacent intervals might have been higher. Because TIC contents are not elevated (1.7–8.1%, mean value 5.6%), precipitation of Mn-carbonate is questionable in these intervals.

Besides increased availability of dissolved Mn, pore volume may influence the potential for precipitation of Mn-bearing minerals during diagenesis. The carbonate-rich layers with elevated Mn contents are visually affected by carbonate diagenesis, e.g. precipitation of calcite (Erbacher et al., 2004). Increased pore volume, either through the occurrence of foraminiferal packstones or of “ash-like” layers, may have favored authigenic formation of Mn-bearing minerals.

3.5.2. Cobalt

Under oxygen depleted conditions like in an OMZ, Mn–and Fe-oxi/hydroxide-associated Co would be mobilized and transported away. In Gulf of California upwelling sediments (Brumsack, 1989) or the Peruvian margin (Böning et al., 2004), Co is depleted similar to Mn. In contrast to Mn, which forms stable sulfides only under very special conditions, Co precipitates as CoS when free hydrogen sulfide is present (Heggie and Lewis, 1984; Gendron et al., 1986).

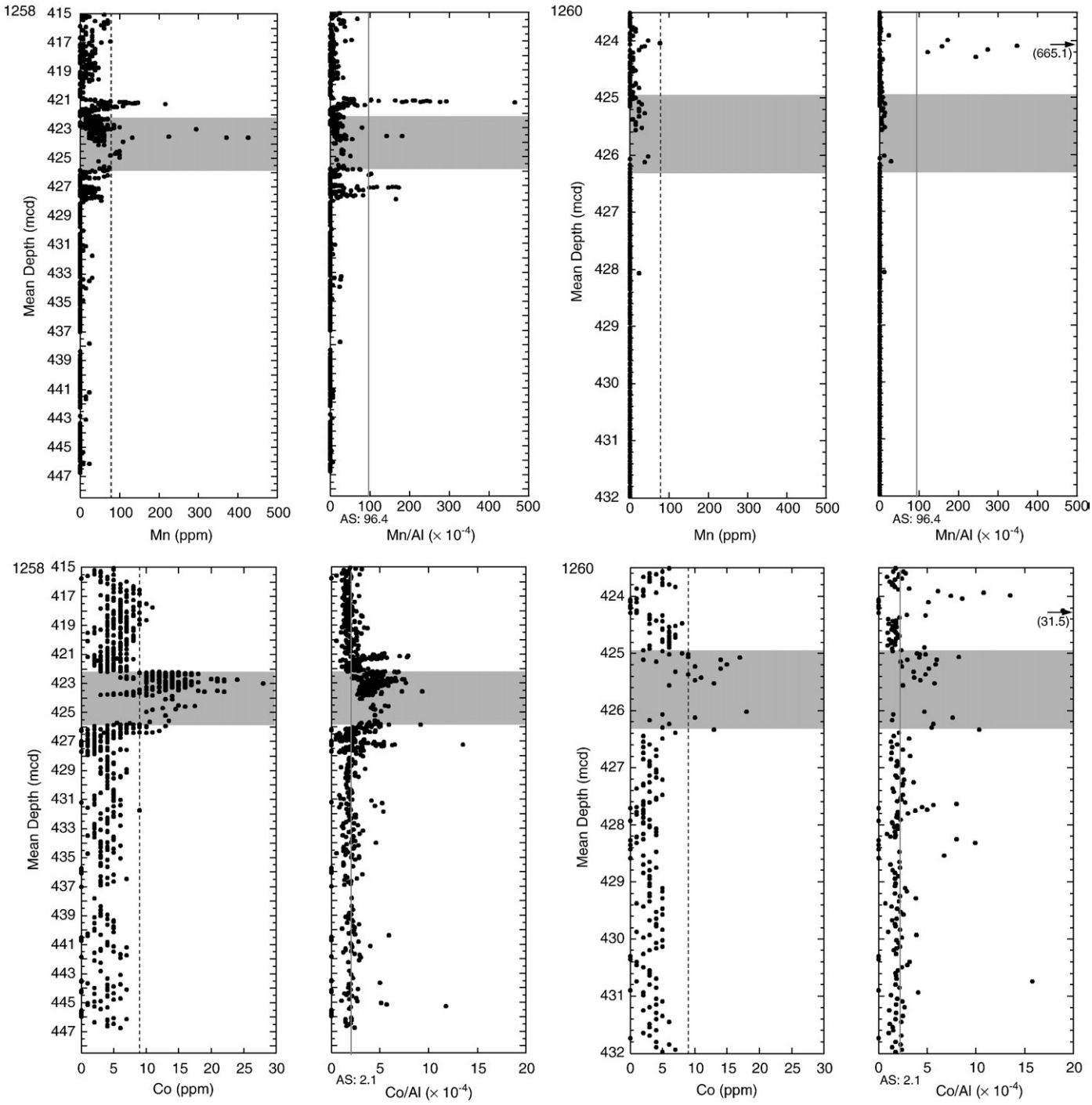

Fig. 9. Depth-profiles for Mn, Mn/Al, Co and Co/Al for Cenomanian/Turonian black shales at Site 1258 and Site 1260. Grey: OAE 2; grey solid line: element/Al ratio of 'average shale' (AS) (Wedepohl, 1971, 1991); dashed line: quantification limit (see Appendix A).

The profiles of Co concentration (Fig. 9) at Site 1258 and Site 1260 show that nearly all sediments below and above OAE 2 are characterized by very low Co concentrations (often below the quantification limit of 9 ppm). Co/Al ratios for Demerara Rise C/T black shales below and above OAE 2 are similar to the Co/Al ratio of average shale (2.1×10^{-4}; Wedepohl, 1971, 1991). Within OAE 2, Co/Al ratios increase to a mean value of 4.4×10^{-4} at both sites with maximum values of 9.4×10^{-4} at Site 1258 and 10.3×10^{-4} at Site 1260.

Thus, the Co distribution is quite similar to the Fe distribution: Under reducing conditions the constant average shale-like value of Co/Al rather indicates fixation of dissolved Co as sulfide than preservation of particulate Co-bearing (hydr)oxide phases. As the Co increase during OAE 2 requires an additional Co-source during deposition, we assume a transport mechanism analogous to Fe from near-shore areas, where reducing but non-sulfidic conditions mobilize additional Co, which is then fixed under truly euxinic conditions further offshore.

3.5.3. Zinc

Cretaceous black shales are known to be highly enriched in Zn. Brumsack (2006) gives a Zn/Al ratio 459×10^{-4} as a C/T mean value ($AS=10.7\times10^{-4}$; Wedepohl, 1971, 1991). Hetzel et al. (2006), found 370×10^{-4} as a mean value of the Cretaceous black shales of Demerara Rise (all sites). The high-resolution study of the C/T interval presented here reveals considerable variability in Zn/Al ratios (Fig. 10). The depth

profile of Site 1258 shows Zn/Al ratios in the same order of magnitude as described by Hetzel et al. (2006) below and above OAE 2 (mean values of 316.0×10^{-4} and 355.9×10^{-4}, respectively; see Table 3). The maxima below and above OAE 2 correspond to maxima in the S_{AVS} profile, indicating the presence of metal sulfides other than pyrite. At Site 1260, the Zn/Al ratios are slightly higher below OAE 2 (mean value 581.4×10^{-4}), while above OAE 2 ratios are lower (mean value 251.1×10^{-4}). At both sites a distinct decrease in Zn/Al ratios during OAE 2 can be observed (mean values 48.1×10^{-4} at Site 1258 and 154.0×10^{-4} at Site 1260).

Addressing the distribution patterns of Co and Zn discussed above we found two different enrichments patterns for these trace metals, both known to be enriched in C/T black shales (Brumsack, 2006) by forming stable sulfides. Whereas C/T black shales from Demerara Rise are enriched in Co during OAE 2, but not before and thereafter, the enrichment in Zn is present throughout the studied interval and displays a rapid decrease in the degree of enrichment within OAE 2.

3.5.4. Molybdenum and vanadium

Overall, element/Al ratios of both Mo and V show clear enrichments in C/T black shales of Demerara Rise (mean $Mo/Al=28.2\times10^{-4}$, $AS=0.15\times10^{-4}$, mean $V/Al=443.8\times10^{-4}$, $AS=14.7\times10^{-4}$; Wedepohl, 1971, 1991; Fig. 10). Mo and V are relatively unreactive in oxic seawater, but are known to be concentrated in sediments overlain by anoxic waters (Brumsack and Gieskes, 1983; Brumsack, 1986).

Vanadium in oxic seawater should be present as V(V). Under moderately reducing conditions, V(IV) forms vanadyl ions (VO^{2-}) that may be removed to the sediment by surface adsorption processes or by formation of organometallic ligands (Emerson and Huested, 1991; Morford and Emerson, 1999). Under more reducing conditions, the presence of free H_2S released by bacterial sulfate reduction causes V to be further reduced to V(III), which can be taken up by geoporphyrins or be precipitated as the solid oxide V_2O_3 or hydroxide $V(OH)_3$ phase (Breit and Wanty, 1991; Wanty and Goldhaber, 1992).

The stable oxidation state of Mo in oxic seawater is Mo(VI). Reduction of Mo(VI) to Mo(IV) and authigenic enrichment in sediments occur under euxinic conditions (Crusius et al., 1996) possibly via diffusion across the sediment–water interface (Emerson and Huested, 1991). Helz et al. (1996) suggested a threshold concentration for H_2S, above which Mo is transformed to particle-reactive thiomolybdates that are scavenged by forming bonds with metal-rich particles, sulfur-rich OM and pyrite.

Tribovillard et al. (2006) addressed the reconstruction of the redox environment of sediments overlain by oxygen-depleted waters via the combined use of different trace metals. While V is reduced and can accumulate under denitrifying conditions, Zn and Mo are enriched mainly under sulfate-reducing conditions. Thus, in the case of V enrichment without Mo enrichment, the authors postulate suboxic/anoxic depositional conditions without free H_2S, whereas sediments exhibiting concurrent enrichments in V and Mo reflect euxinic conditions at the sediment–water interface or in the water column (Algeo and Maynard, 2004; Tribovillard et al., 2004). As the C/T black shales of Demerara Rise are clearly enriched in both, Mo and V, this simplified distinctive feature would hint to euxinic conditions for the depositional environment.

From positive correlations of Mo with sulfurized OM in ancient marine black shales, Tribovillard et al. (2004) emphasized Mo trapping by sulfur-rich OM. No correlation of Mo with pyrite accumulation could be found. Instead, the reduced availability of reactive Fe may favor Mo accumulation, as significant OM sulfurization is only possible when reactive iron is limited. As shown above, we find iron-limitation in most of the studied intervals and an enhanced OM sulfurization during OAE 2. Following the arguments of Tribovillard et al. (2004), we would expect an increase in Mo enrichment during OAE 2. Instead, a clear decrease is visible, implying that other factors influenced Mo accumulation as well. Probably, the concentration of dissolved sulfide in the water column that affected aqueous Mo speciation may have influenced the efficiency of Mo fixation (Neubert et al., in press).

For anoxic basins, Emerson and Huested (1991) showed that the concentrations of Mo and V in the water column are usually lower than in oxic seawater due to their uptake into highly anoxic sediments. As no systematic relationship between the deep-water Mo or V concentrations and H_2S content was found, the authors concluded that concentrations of Mo and V are rather controlled by their flux to sediments and water renewal from outside the basins than by changes in water column anoxia. Algeo and Lyons (2006) analyzed Mo–TOC relationships in sediments from anoxic environments characterized by different degrees of hydrographic restriction. In silled anoxic basins, decreasing Mo/TOC ratios with increasing degree of restriction imply that sedimentary Mo concentrations were controlled by Mo availability from the overlying water column, and thus by resupply of Mo via deepwater renewal. Algeo and Lyons (2006) termed this drawdown of Mo concentrations in deep water during stagnant intervals the “basin reservoir effect”.

Fig. 11 shows Mo/TOC profiles as well as X–Y-plots of Mo versus TOC. Mo/TOC values vary between $\sim5\times10^{-4}$ and $\sim20\times10^{-4}$ for sediments deposited before OAE 2. Similar to Mo/Al, Mo/TOC ratios decrease rapidly at the onset of OAE 2, staying low during OAE 2, before a slight increase is visible after OAE 2. The slopes of regression lines for X–Y-plots of Mo versus TOC give similar low Mo/TOC ratios for samples within the OAE 2 interval at both sites (2.3×10^{-4} at Site 1258 and 2.4×10^{-4} at Site 1260). These values are even lower than the value of $Mo/TOC=4.5\pm1\times10^{-4}$ reported by Algeo and Lyons (2006) for the Black Sea. Regression lines for samples deposited before OAE 2 give Mo/TOC values of 10.7×10^{-4} at Site 1258 and 8.8×10^{-4} at Site 1260. The increase in Mo/TOC ratios after OAE 2 is less pronounced at Site 1260 ($Mo/TOC=5.2\times10^{-4}$) than at Site 1258 ($Mo/TOC=9.4\times10^{-4}$).

As V burial under anoxic conditions is also known to be linked to OM (Breit and Wanty, 1991; Emerson and Huested, 1991; Morford and Emerson, 1999), we analyzed V/TOC ratios analogues to Mo and Zn/S_T ratios as Zn is known to form stable sulfides if H_2S is present (Jacobs et al., 1985) (Fig. 11). Both, V and Zn, show the distinct decrease relative to TOC and S_T during OAE 2 pointing to decoupling of OM burial, sulfidization and TM availability during OAE 2.

Fig. 12 shows the enrichment factors relative to average shales for Fe_T, Co, Mo, V and Zn for Sites 1258 and 1260, and for C/T mean values (Brumsack, 2006). The enrichment factor for Fe_T is ~1 at Site 1258 below and above the CTBE and at Site 1260 below the CTBE, indicating Fe/Al ratios similar to average shale. The observed enrichment in sediments of Site 1260 above the CTBE may be an artefact owing to normalization of values close to the Fe and Al detection limit in carbonate-rich sediments (see Fig. 4, ~424 mcd). As described above, the distribution patterns of Co are similar to those of Fe_T.

Zn, Mo and V show similar enrichment patterns, with highest values below, intermediate values above, and lowest values within OAE 2. At Site 1258, Mo, V and Zn are enriched to similar degrees below and above OAE 2. The decline of enrichment during OAE 2 is more pronounced than for Site 1260. Overall, the degrees of enrichment of Mo, V and Zn are similar to other C/T sediments listed by Brumsack (2006). Only the sediments deposited during OAE 2 at Site 1258 are characterized by less pronounced Mo, V and Zn enrichments relative to other C/T black shales.

In summary, we suggest two important mechanisms affecting Fe_T and trace metal distribution patterns in C/T black shales at Demerara Rise:

Locally, Mn depletion hints to reducing conditions an open-marine environment, e.g. an OMZ. Fe_T and Co enrichments during OAE 2 indicate an expansion of this OMZ. As their seawater concentrations are generally low, at least part of the sedimentary Fe_T and Co enrichments during OAE 2 must be due to mobilization from oxygen-depleted nearshore-sediments. Whereas Fe and Co are conveyed along with Mn in suboxic waters, they will be precipitated as sulfides when hydrogen sulfide is present in the water column.

Regarding the source for TMs enriched in TOC-rich sediments, Mo and V are highly concentrated in seawater, and they may have become enriched in the sediment via diffusion from the water column. As extreme Zn enrichments in Cretaceous black shales (compared to

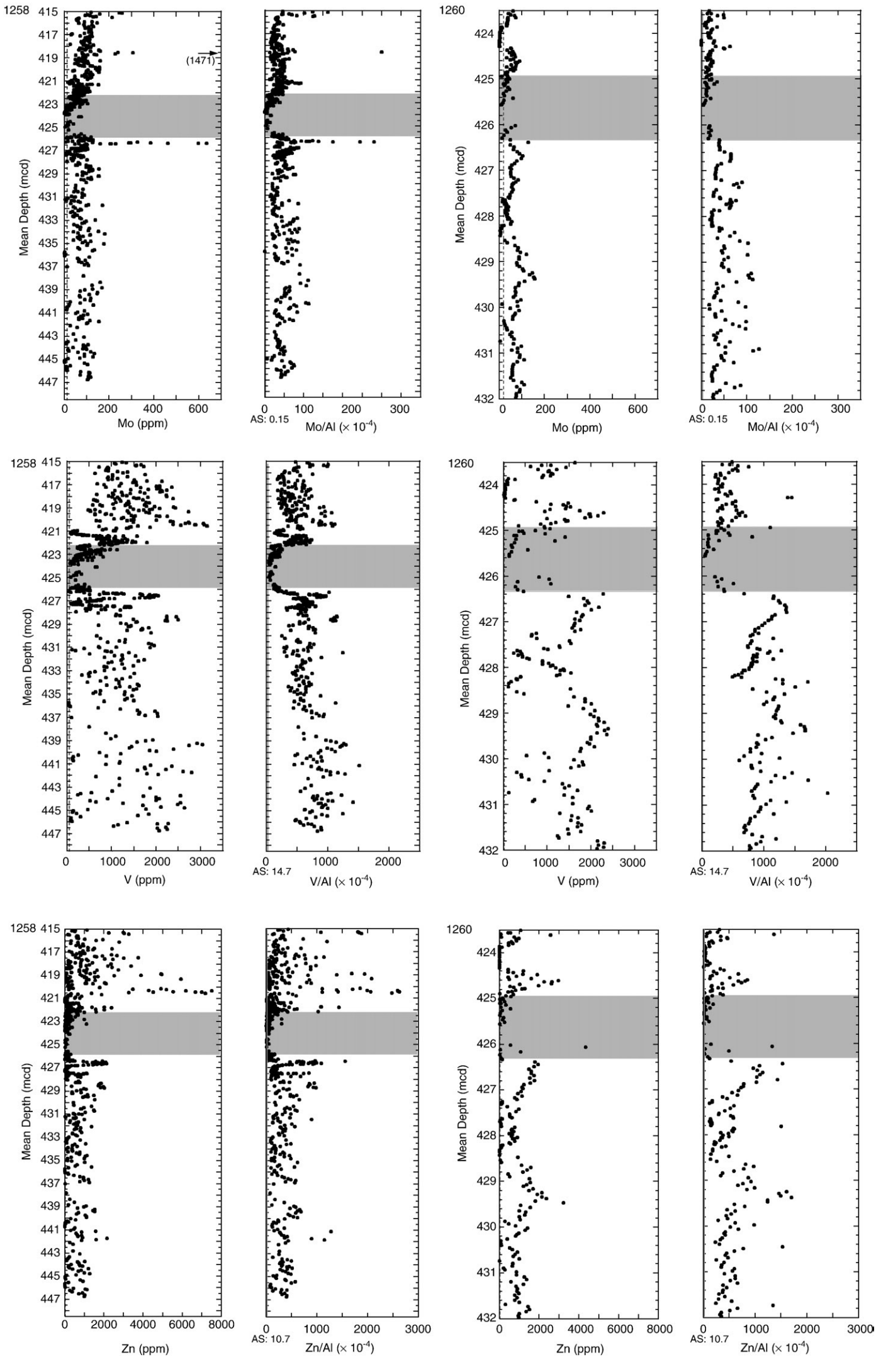

Fig. 10. Depth-profiles for Mo, Mo/Al, V, V/Al, Zn and Zn/Al for Cenomanian/Turonian black shales of Site 1258 and Site 1260. Grey: OAE 2; grey solid line: element/Al ratio of 'average shale' (AS) (Wedepohl, 1971, 1991); dashed line: quantification limit (see Appendix A).

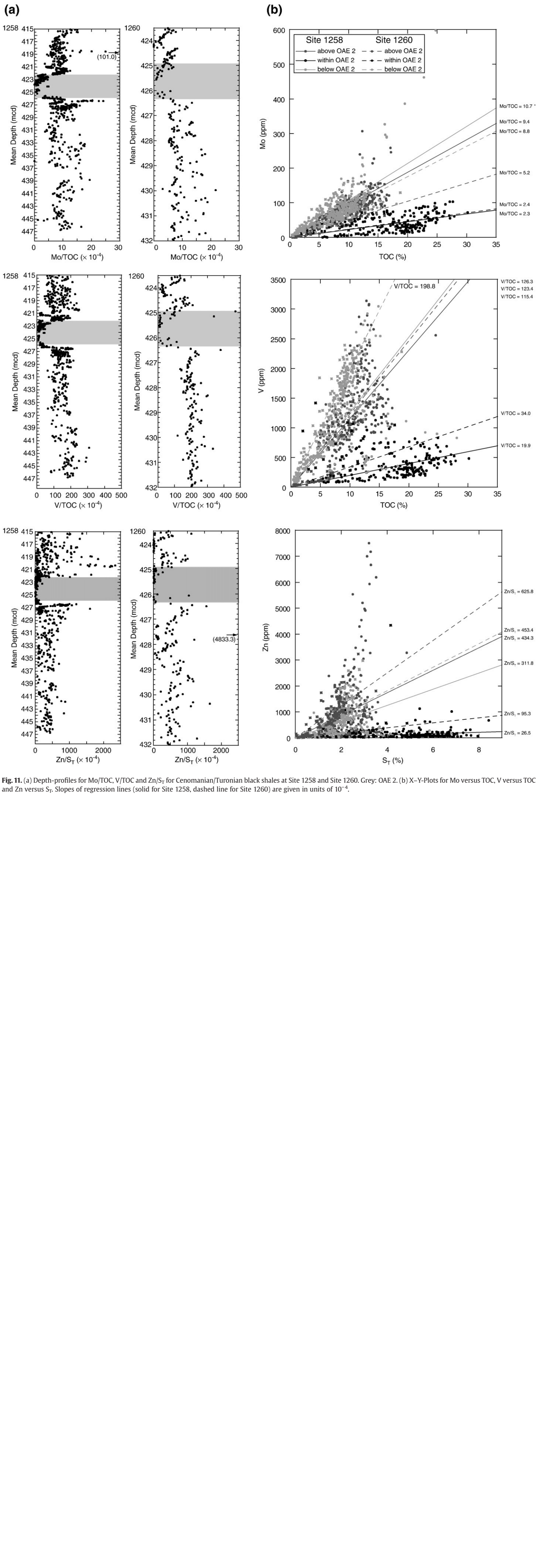

Fig. 11. (a) Depth-profiles for Mo/TOC, V/TOC and Zn/S_T for Cenomanian/Turonian black shales at Site 1258 and Site 1260. Grey: OAE 2. (b) X–Y-Plots for Mo versus TOC, V versus TOC and Zn versus S_T. Slopes of regression lines (solid for Site 1258, dashed line for Site 1260) are given in units of 10^{-4}.

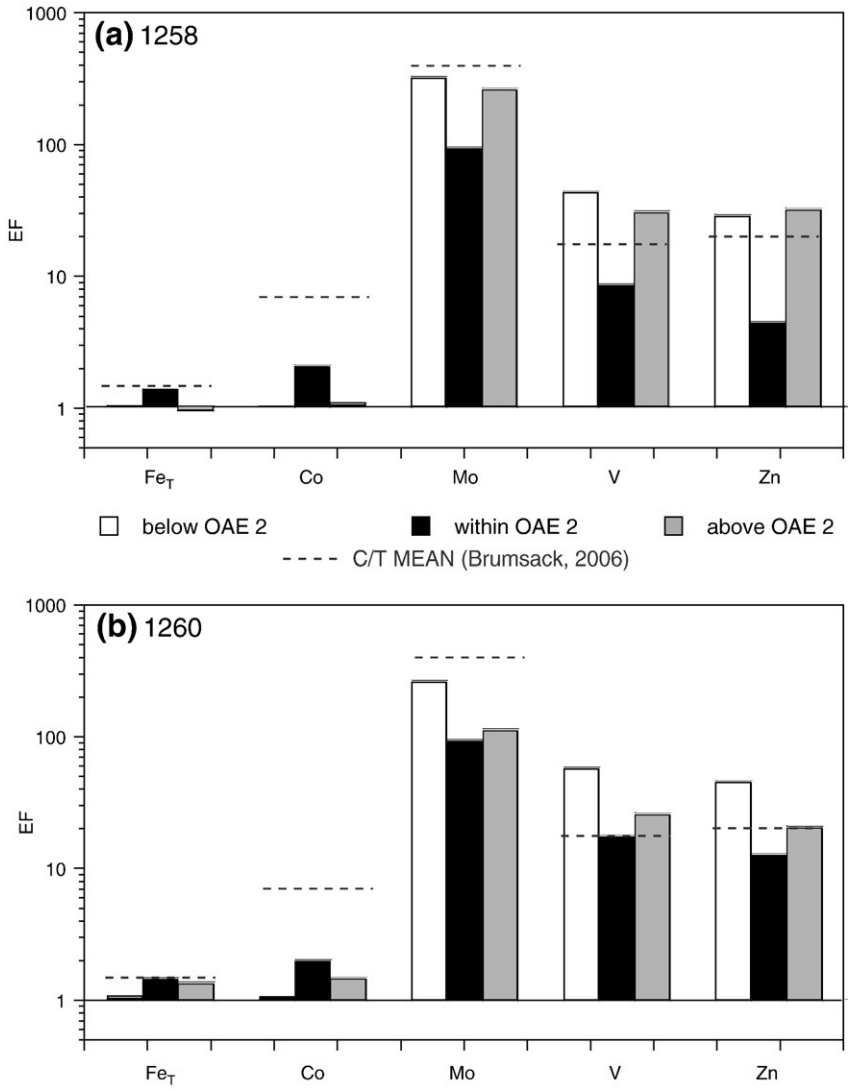

Fig. 12. Mean enrichment factors (EF) of Fe_T, Co, Mo, V and Zn relative to 'average shale' (AS) (Wedepohl, 1971, 1991) for Cenomanian/Turonian black shales at Demerara Rise. EF = element/Al(sample)/element/Al(AS). (a) Site 1258, (b) Site 1260. Dashed lines: EF for C/T mean values (Brumsack, 2006).

recent TOC-rich sediments) require an additional Zn source, a higher seawater concentration of Zn due to hydrothermal input during the Cretaceous seems likely (Arthur et al., 1988; Brumsack, 2006). Under such conditions seawater might again be the dominating source for Zn enrichments. Thus, on a larger if not global scale, we emphasize a decline in seawater TM availability during OAE 2, revealed by the decrease in Mo, V and Zn enrichment.

Taking seawater as the dominant source for Mo, V and Zn, the depletion in TM/Al may reflect the global onset of black shale deposition during OAE 2 and the rapid drawdown of the seawater TM reservoir by the spreading of euxinic depositional areas. In the modern oceans, only 0.2% of the seafloor are hypoxic (Helly and Levin, 2004), while during the Cretaceous, particularly during OAE 2, such conditions were much more wide-spread. Kuypers et al. (2002) pointed out that the proto-North Atlantic Ocean was one of the main sites of carbon burial during OAE 2. Paleogeographic reconstructions show that the proto-North Atlantic Ocean was a restricted area with major seawater supply coming from the Tethys only. The black shales deposited in the Tethys and in the proto-North Atlantic Ocean during OAE 2 (e.g. Kuhnt et al., 1990) definitely formed a significant TM sink. We therefore assume that the decline in TM enrichment seen at Demerara Rise indicates a drawdown of TMs from seawater, similar to the "basin reservoir effect" described by Algeo and Lyons (2006).

3.6. Productivity proxies

Fig. 13 show the enrichments factors for some elements, used for approximation of paleoproductivity.

Phosphorus belongs to the essential nutrient elements controlling marine primary productivity (e.g. Broecker and Peng, 1982). High concentrations are found in recent upwelling sediments pointing towards enhanced nutrient supply and resulting high bioproductivity (e.g., Böning et al., 2004). Incorporated into organic material (e.g. in marine phytoplankton; Redfield, 1958) P is deposited in the sediment, where it is preferentially remineralized relative to TOC and liberated to the pore water and maybe forming authigenic phosphatic precipitates. Under oxygen-depleted conditions, when potential phosphate scavengers such as Fe-(hydr)oxides are reduced and not available, organic P release in sediments is even higher. Therefore, in TOC-rich sediments deposited under anoxic conditions the TOC/P ratio should be increased (Ingall et al., 1993 and references therein).

Nederbragt et al. (2004) concluded from measurements of total phosphorus and organic carbon in C/T sediments from the Tarfaya Basin, Morocco, that the main underlying mechanism that allowed and sustained enhanced carbon burial during the mid-Cretaceous was a perturbation of the oceanic phosphorus cycle. More effective regeneration of organic phosphorus under anoxic conditions can lead to an increase in

dissolved oceanic phosphate, which in turn stimulates surface-water productivity (Ingall et al., 1993; Bjerrum and Canfield, 2002; Mort et al., 2007). The Shipboard Scientific Party (2004) describes the presence of P-rich concretions in black shales of Demerara Rise. Fig. 13 shows a clear enrichment of P relative to average shale in the sections studied. This points towards a high primary productivity comparable to coastal upwelling areas. The minor enrichment during OAE 2 hints to a decreasing nutrient supply or to partial loss of P during at least periodically truly anoxic conditions in comparison to the situation before and thereafter.

The non-lithologenic excess barium has been interpreted as a paleoproxy for bio-productivity (Schmitz, 1987; Dymond et al., 1992; Paytan et al., 1996). These biogenic barites ($BaSO_4$) (Bishop, 1988; Bertram and Cowen, 1997; Paytan et al., 2002; Bernstein and Byrne, 2004) are only stable under seawater sulfate concentrations (Church and Wohlgemuth, 1972). Due to the microbial sulfate reduction in TOC-rich sediments, barite may be dissolving, leading to the mobilization of Ba (Brumsack and Gieskes, 1983; McManus et al., 1998; Eagle et al., 2003). Authigenic barite may precipitate at the top of the sulfate-depletion zone forming diagenetic barite fronts within or above TOC-rich strata (Torres et al., 1996; Bréhéret and Brumsack, 2000).

Hetzel et al. (2006) found the highest Ba/Al above the Cretaceous black shales, while within the black shales Ba/Al ratios are still high despite of the present absence of sulfate in the pore waters (Erbacher et al., 2004). Arndt et al. (2006) showed in a transport-reaction model that not only OM degradation but also anaerobic oxidation of methane (AOM) above the black shales of Demerara Rise influences sulfate availability and therefore the remobilization of biogenic barium. These authors further showed that temporal dynamics of degradation processes caused various shifts of the barite precipitation zone during burial, thus inhibiting the formation of an authigenic barite front or causing the dissolution of earlier formed fronts.

Fig. 13 shows an enrichment of Ba similar to the C/T mean values from Brumsack (2006). This enrichment indicates elevated primary productivity during deposition. But a large fraction of former barite may have been remobilized and formed diagenetic barites above the black shales. For this reason the use of Ba as a paleoproxy on a quantitative level (Dymond et al., 1992) for Cretaceous settings in such an environment is highly questionable.

4. Paleoenvironmental implications and comparison with other paleoproxies

The paleoconditions for the depositional environment based on geochemical arguments are summarized in Fig. 14. From analysis of TOC–Fe–S systematics and TM distribution patterns we can conclude that a depositional environment with an expanded oxygen-minimum-zone (OMZ) similar to coastal upwelling areas existed before the onset of OAE 2 (Fig. 14a). Enrichments of TOC, P and Ba hint to enhanced bioproductivity. The depletion in Mn and enrichment in redox-sensitive

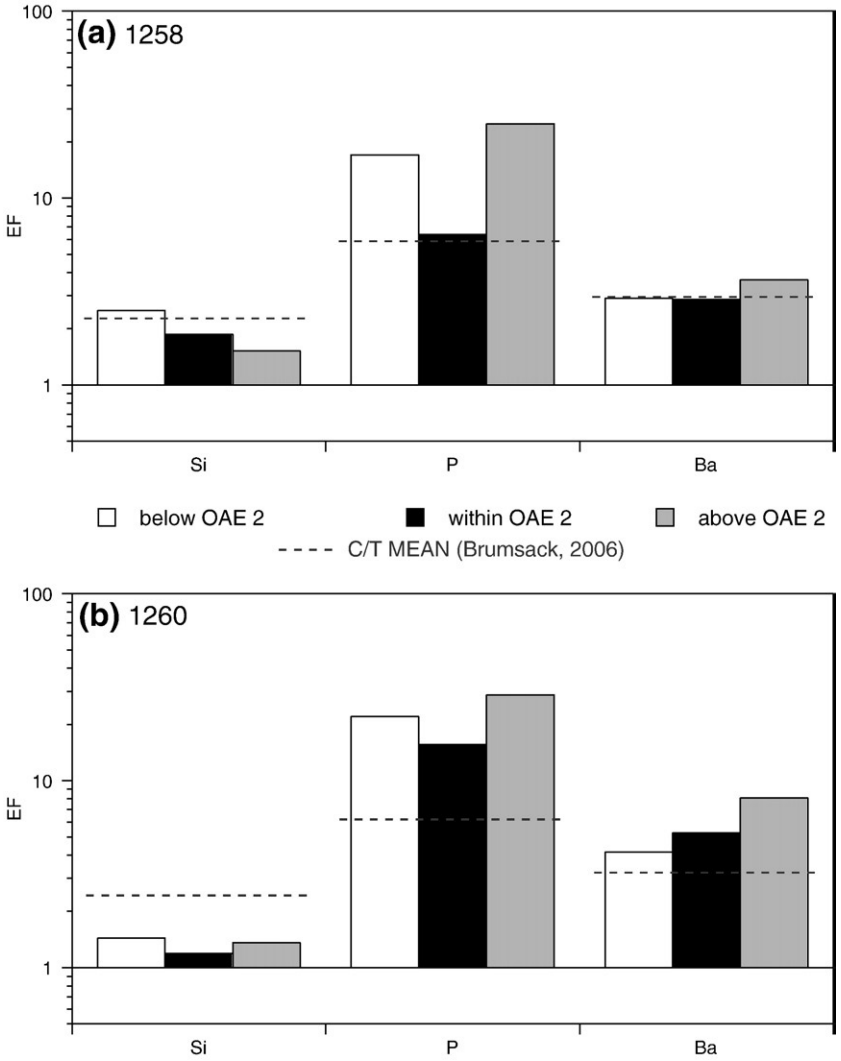

Fig. 13. Mean enrichment factors (EF) of Si, P and Ba relative to 'average shale' (AS) (Wedepohl, 1971, 1991) for Cenomanian/Turonian black shales at Demerara Rise. EF=element/Al (sample)/element/Al(AS). (a) Site 1258, (b) Site 1260. Dashed lines: EF for C/T mean values (Brumsack, 2006).

TM indicate at least suboxic conditions. During OAE 2, an increase in the Fe_P/Fe_T ratio points to the rapid development of truly euxinic conditions with free hydrogen-sulfide in the water column (Fig. 14b). This is confirmed by a rise in Fe_T/Al and Co/Al ratios. An expansion of the OMZ, possible due to intensified paleoproductivity and/or sea level rise, leads to mobilization of Fe and Co from nearshore sediments. Thus, enrichment in Fe_T and Co in the sediments is possible, when hydrogen sulfide is present in the water column for sulfide precipitation.

Musavu-Moussavou and Danelian (2006) analyzed the radiolarian abundances across OAE 2 at Site 1258 and Site 1261. The presence of radiolarians at Site 1258 and to a lesser degree at the shallower Site 1261 below OAE 2 indicates, at least periodically, oxygenated surface waters. During OAE 2, the absence of radiolarians at Site 1261 and only rare occurrence at Site 1258 hint at the intensification of euxinic conditions, while above OAE 2 radiolarians are present again, this time with higher abundances at Site 1261 than at Site 1258. In marine sediments Si derives either from the terrigenous detritus as alumino-silicates, quartz or from a biogenous opal from siliceous plankton (diatoms or radiolarians; Brumsack, 1989). Assuming an 'average shale'-like terrigenous background for C/T-black shales of Demerara Rise the enrichment in Si indicates the presence of additional Si other than present in the clay component. Owing to the absence of heavy mineral related elements Hetzel et al. (2006) could exclude the presence of excess quartz in Cretaceous black shales of Demerara Rise and instead assumed a biogenous origin for the excess silica. We suppose that the enrichment in Si shown in Fig. 13 represents Si derived from radiolarian tests. The general pattern with slight enrichment of Si below and above OAE 2 fits well with the findings of Musavu-Moussavou and Danelian (2006).

Hardas and Mutterlose (2007) analyzed the calcareous nannofossil assemblages of Site 1258 and 1260. They found highest absolute abundances below OAE 2 at both sites. During OAE 2 the absolute abundance decreases and also the species assemblages change. From the now dominating species the authors conclude a higher bio-productivity. Instead of cooler temperatures, as suggested by Forster et al. (2007) at Site 1260 within OAE 2, Hardas and Mutterlose (2007) postulate a slight increase in sea surface temperatures. They suggest a possible breakdown of water column stratification and thus a shallowing of the

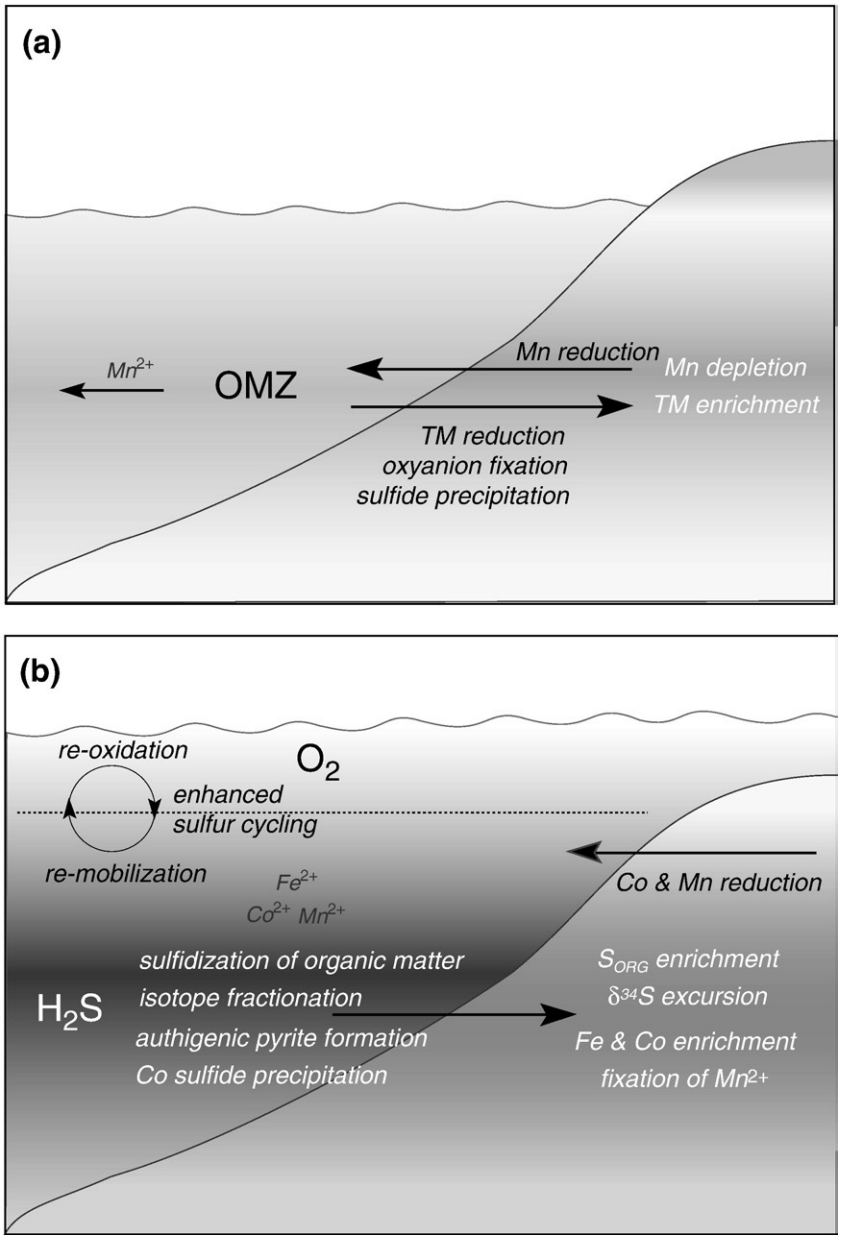

Fig. 14. Simplified scheme of paleoenvironmental conditions as deduced from geochemical data before/after (a) and during (b) OAE 2.

nutricline. This fits into a picture of a euxinic water column and the decline in total abundance of nannofossils.

Regarding the redox conditions at the sediment–water interface Friedrich et al. (2006) suggest a strengthening of the OMZ during OAE 2, based on the benthic foraminifera assemblage at Sites 1258–1261.

Below OAE 2 the authors suggest anoxic to sometimes slightly dysoxic bottom-water conditions at the shallower sites, whereas for the deepest Site 1258 more oxygenated but still dysoxic bottom waters were proposed, possibly due its position below the OMZ. During OAE 2, the total absence of benthic foraminifera hints to anoxic conditions, but short-term re-populations may indicate bottom-water oxygenation. The authors find these events in the lower third of OAE 2 at all sites studied. Forster et al. (2007) correlate these occurrences with a cooling event at Site 1260. Benthic foraminiferal assemblages indicate continued oxygen-deficient bottom-water conditions following OAE 2 with the exception of one short-term increase in oxygenation immediately above the OAE 2. After ~0.5 Ma. more oxygenated bottom-water masses are postulated.

From geochemical data we suppose euxinic conditions during OAE 2. The presence of benthic foraminifera indicates that the euxinic conditions may not have been permanent. Evidence for the short-term complete re-oxidation of the bottom water is not given by the geochemical data, although peaks in Mn/Al several decimeters above the repopulation events of benthic foraminifera at Site 1258 may indicate a shallowing of the OMZ thus introducing Mn to the sediment.

Addressing the same questions by different paleo-proxies may lead to different results under certain circumstances. If sedimentation rates are low, and the amount of sample material required for certain analyses comprises a time-span in which several changes in depositional environment may have occurred, the chemical result would be an integrated signal due to homogenization of the sample. In contrast, analyzing fossils might give only a snapshot of paleoconditions. Contrasting results for the same intervals may therefore hint to unstable conditions. Forster et al. (2007) suggest such unstable conditions during OAE 2 at Site 1260. From our point of view a closer look is necessary, if and to what extent the presence of the "ash-like" layers, which were omitted here, may influence directly or by diagenetic effects results obtained in close vicinity to these layers.

5. Summary and conclusions

From geochemical analysis the following conclusions regarding the depositional environment of C/T black shales at Demerara Rise during OAE 2 can be drawn:

- Elevated Fe_P/Fe_T, Fe_T/Al, and Co/Al values within the OAE 2 confirm euxinic conditions but, at the same time, require a zone where reducing but non-sulfidic conditions enable Fe and Co mobilization in oxygen depleted nearshore sediments.
- The existence of an expanded oxygen-minimum-zone (OMZ) is demonstrated by extremely low Mn/Al ratios. Elevated Mn/Al ratios are only seen in distinct horizons. Overgrowth of Mn-carbonates on pre-existing carbonate tests seems to be possible under euxinic conditions and elevated pore water alkalinities.
- Mo/Al, V/Al and Zn/Al ratios are generally high throughout the investigated sequence, but a significant depletion is notable exactly during OAE 2. The decrease in enrichment for these seawater derived trace metals may reflect the global onset of black shale deposition during OAE 2 and the rapid drawdown of the seawater TM reservoir by the enlargement of euxinic depositional areas.
- The enrichment in phosphorus and barium points towards high bio-productivity like in recent upwelling areas. Due to diagenesis driven by the reducing conditions a quantitative interpretation is not possible.
- Besides fixation of sulfide as iron sulfide, organic matter acts as an important sulfur trap during early diagenesis. During OAE 2 the amounts of both, pyrite and organically bound sulfur increase. A negative shift in the stable sulfur isotope curve during OAE 2 indicates changes in the overall sulfur cycle, similar to results observed previously in the Tarfaya Basin.

According to the assumed high bioproductivity and the depletion in Mn, the C/T black shales of Demerara Rise are compatible with a situation encountered in modern coastal upwelling areas within an expanded OMZ. During OAE 2 a more euxinic situation was established with the presence of free hydrogen sulfide in the water column.

Acknowledgements

We would like to thank the crew and scientific party of ODP Leg 207 for their kind support. This research used samples and/or data provided by the Ocean Drilling Program (ODP). ODP is sponsored by the U.S. National Science Foundation (NSF) and participating countries under management of Joint Oceanographic Institutions (JOI), Inc. This contribution has benefited from the thorough reviews by Tim Lyons and an anonymous reviewer. AH is grateful to Astrid Forster and Christian März for valuable discussions, Knut Bernhardt for performing time series analysis and Imke Notholt for EDX assistance. MEB wishes to thank Andrea Schipper for technical assistance and E. Clapton, N. Futado, C. Hynde, and J. Stone for acoustical inspiration during work on the manuscript. This study was funded by Deutsche Forschungsgemeinschaft (IODP-SPP grants BR 775/16+17; BO 1584/2) and by Max Planck Society, Germany.

Appendix A

Quantification limit, precision and accuracy of analyzed elements

Element	Method	Quantification limit	Precision SD (1σ) (rel%)	Accuracy (rel%)
S_T	IR-analyzer	0.56%	3.0	99.9
TC	IR-analyzer	1.22%	1.6	101.2
TIC	Coulometry	0.19%	2.3	99.8
Si	XRF	1.94%	1.3	99.1–101.0
Ti	XRF	0.03%	1.2	98.1–101.0
Al	XRF	0.77%	1.6	98.7–100.6
Fe_T	XRF	0.33%	1.2	98.7–100.6
Mg	XRF	0.26%	1.9	99.3–101.0
Ca	XRF	0.80%	1.6	99.4–99.7
Na	XRF	0.21%	5.7	90.1–100.6
K	XRF	0.20%	2.6	95.5–100.4
P	XRF	0.04%	6.5	98.6–108.8
As	XRF	4 ppm	7.0	96.0–100.0
Ba	XRF	77 ppm	2.5	98.8–102.6
Co	XRF	9 ppm	8.1	93.7–95.4
Cr	XRF	17 ppm	2.9	98.4–104.4
Cu	XRF	21 ppm	6.6	94.0–102.2
Mn	XRF	78 ppm	2.2	97.5–103.1
Mo	XRF	14 ppm	6.0	94.1–104.3
Ni	XRF	14 ppm	3.3	99.1–103.8
Rb	XRF	26 ppm	3.9	92.7–101.8
Sr	XRF	120 ppm	9.7	101.0–102.2
U	XRF	5 ppm	10.9	109.0–110.2
V	XRF	56 ppm	4.2	99.8–100.9
Y	XRF	8 ppm	5.4	98.5–109.5
Zn	XRF	33 ppm	3.9	95.1–102.4
Zr	XRF	30 ppm	3.6	96.1–103.7

For stable isotope measurements, see section on Materials and methods.

Notes: Procedures and accuracy of all methods were checked with in-house reference materials (IR-Analyzer: PS-S (n=286); coulometry: Loess (n=387); XRF: DR-BS (n=33), TW-TUC (n=14) and PS-S, (n=11)). Quantification limit is defined as 6 times the maximum standard deviation (1σ). Precision is defined as 100% times the best estimate standard deviation (1σ) divided by the mean of the repeats. The maximum value is given. SD=standard deviation. Accuracy is defined as 100% times the mean of the repeat analyses divided by the expected value. For XRF the range of different reference material is given.

Appendix B. Identification of so-called "ash layers" (see text for details)

(a) Profiles for Si/Al, Ti/Al and K/Al for Cenomanian/Turonian black shales at Sites 1258 and 1260. Grey: OAE 2; dashed line: "ash layers". (b) Images of sediment intervals (available online from Erbacher et al., 2004, doi:10.2973/odp.proc.ir.207.2004). Dashed line: "ash layers".

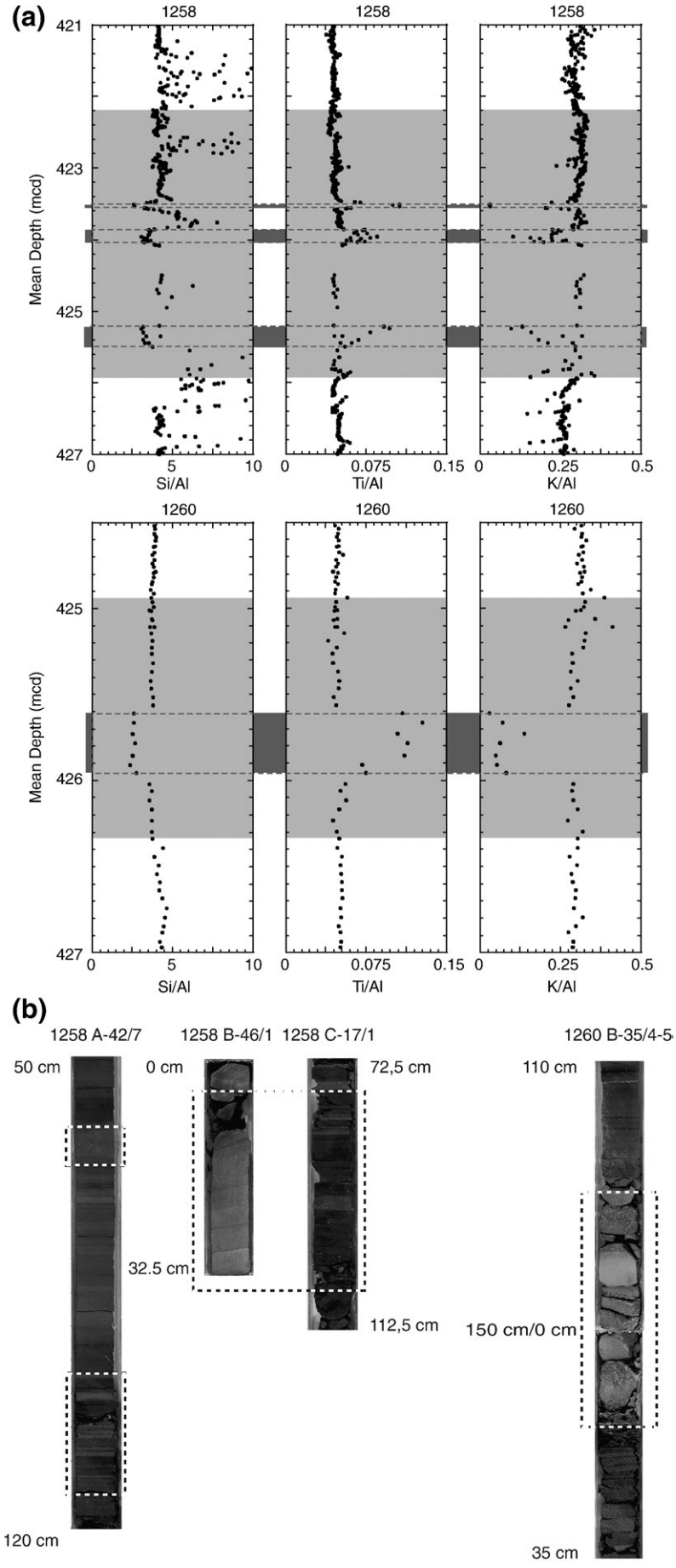
(a)
1258
1258
1258
421
423
425
427
Mean Depth (mcd)
0
5
10
Si/Al
0
0.075
0.15
Ti/Al
0
0.25
0.5
K/Al
1260
1260
1260
425
426
427
Mean Depth (mcd)
0
5
10
Si/Al
0
0.075
0.15
Ti/Al
0
0.25
0.5
K/Al
(b)
1258 A-42/7
1258 B-46/1
1258 C-17/1
1260 B-35/4-5
50 cm
120 cm
0 cm
32.5 cm
72,5 cm
112,5 cm
110 cm
150 cm/0 cm
35 cm

(c) Comparison of average element contents and element/Al ratios of omitted samples (unknown source. secondary overprinted)

		Omitted samples (n=34)	Average C/T black shales Demerara Rise	Average shale (Wedepohl, 1971, 1991)
S_T	%	6.03	2.60	0.24
S_P	%	(n=11) 1.67	0.79	
$\delta^{34}S_P$	‰	(n=4) −15.4	−15.8	
TIC	%	2.73	5.56	0.35
TOC	%	8.55	10.39	
Si	%	14.69	10.26	27.53
Ti	%	0.36	0.10	0.46
Al	%	4.60	2.16	8.84
Fe_T	%	4.36	1.27	4.80
Mg	%	1.01	0.51	1.60
Ca	%	10.26	19.61	1.57
Na	%	1.25	0.88	1.19
K	%	0.74	0.64	2.99
P	%	0.08	0.33	0.07
As	ppm	54	20	10
Ba	ppm	511	524	580
Co	ppm	23	6	19
Cr	ppm	136	113	90
Cu	ppm	152	63	45
Mn	ppm	332	17	850
Mo	ppm	32	58	1
Ni	ppm	132	131	68
Rb	ppm	22	25	140
Sr	ppm	564	771	300
U	ppm	7	15	4
V	ppm	530	907	130
Y	ppm	17	20	41
Zn	ppm	209	608	95
Zr	ppm	35	33	160
$S_{T\ cf}$	%	12.10	4.94	0.25
TOC_{cf}	%	2.27	19.86	
S_T/Al		32.18	1.35	0.03
TOC/Al		89.00	5.40	0.02
Si/Al		3.18	5.13	
Ti/Al		0.08	0.05	0.05
Fe_T/Al		0.96	0.65	0.54
Mg/Al		0.31	0.53	0.18
Ca/Al		12.03	39.54	0.18
Na/Al		0.27	0.47	0.13
K/Al		0.17	0.32	0.34
P/Al		0.02	0.15	0.01
As/Al	$\times 10^{-4}$	12.9	11.2	1.1
Ba/Al	$\times 10^{-4}$	122.6	294.4	65.6
Co/Al	$\times 10^{-4}$	5.1	3.1	2.1
Cr/Al	$\times 10^{-4}$	30.6	52.3	10.2
Cu/Al	$\times 10^{-4}$	32.6	33.8	5.1
Mn/Al	$\times 10^{-4}$	80.4	15.5	96.2
Mo/Al	$\times 10^{-4}$	6.2	31.9	0.1
Ni/Al	$\times 10^{-4}$	28.3	67.5	7.7
Rb/Al	$\times 10^{-4}$	4.8	11.1	15.8
Sr/Al	$\times 10^{-4}$	197.9	693.6	33.9
U/Al	$\times 10^{-4}$	2.4	11.3	0.4
V/Al	$\times 10^{-4}$	119.0	498.0	14.7
Y/Al	$\times 10^{-4}$	5.2	11.7	4.6
Zn/Al	$\times 10^{-4}$	49.4	284.4	10.7
Zr/Al	$\times 10^{-4}$	10.4	20.1	18.1

Cenomanian/Turonian black shales of Demerara Rise (mean values of Table 3–5) and 'average shale'.

References

Algeo, T.J., Lyons, T.W., 2006. Mo-total organic carbon covariation in modern anoxic marine environments: implications for analysis of paleoredox and paleohydrographic conditions. Paleoceanography 21, PA1016.

Algeo, T.J., Maynard, J.B., 2004. Trace element behavior and redox facies in core shales of the Upper Pennsylvanian Kansas-type cyclothems. Chemical Geology 206 (3–4), 289–318.

Arndt, S., Brumsack, H.-J., Wirtz, K., 2006. Cretaceous black shales as active bioreactors: a biogeochemical model for the deep biosphere encountered during ODP Leg 207 (Demerara Rise). Geochimica et Cosmochimica Acta 70 (2), 408–425.

Arthur, M.A., Schlanger, S.O., Jenkyns, H.C., 1987. The Cenomanian/Turonian Oceanic Anoxic Event, II. Palaeoceanographic controls on organic-matter production and preservation. In: Brooks, J., Fleet, A.J. (Eds.), Marine Petroleum Source Rocks. Special Publication, 26. Geological Society, London, pp. 401–420.

Arthur, M.A., Dean, W.E., Pratt, L.M., 1988. Geochemical and climatic effects of increased marine organic carbon burial at the Cenomanian/Turonian boundary. Nature 335 (6192), 714–717.

Berner, R.A., Raiswell, R., 1983. Burial of organic carbon and pyrite sulfur in sediments over Phanerozoic time: a new theory. Geochimica et Cosmochimica Acta 47 (5), 855–862.

Bernstein, R.E., Byrne, R.H., 2004. Acantharians and marine barite. Marine Chemistry 86 (1–2), 45–50.

Bertram, M.A., Cowen, J.P., 1997. Morphological and compositional evidence for biotic precipitation of marine barite. Journal of Marine Research 55 (3), 577–593.

Bishop, J.K.B., 1988. The barite–opal–organic carbon association in oceanic particulate matter. Nature 332 (6162), 341–343.

Bjerrum, C.J., Canfield, D.E., 2002. Ocean productivity before about 1.9 Gyr ago limited by phosphorus adsorption onto iron oxides. Nature 417 (6885), 159–162.

Böning, P., Brumsack, H.-J., Böttcher, M.E., Schnetger, B., Kriete, C., Kallmeyer, J., Borchers, S.L., 2004. Geochemistry of Peruvian near-surface sediments. Geochimica et Cosmochimica Acta 68 (21), 4429–4451.

Böttcher, M.E., 1997. The transformation of aragonite to $Mn_xCa_{(1-x)}CO_3$ solid-solutions at 20 °C: an experimental study. Marine Chemistry 57 (1–2), 97–106.

Böttcher, M.E., Rinna, J., Warning, B., Wehausen, R., Howell, M.W., Schnetger, B., Stein, R., Brumsack, H.-J., Rullkötter, J., 2003. Geochemistry of sediments from the connection between the western and eastern Mediterranean Sea (Strait of Sicily, ODP Site 963). Palaeogeography, Palaeoclimatology, Palaeoecology 190, 165–194.

Böttcher, M.E., Jørgensen, B.B., Kallmeyer, J., Wehausen, R., 2004. S and O isotope fractionation in the western Black Sea. Geochimica et Cosmochimica Acta 68, A345.

Böttcher, M.E., Hetzel, A., Brumsack, H.-J., Schipper, A., 2006. Sulfur–iron–carbon geochemistry in sediments of the Demerara Rise. In: Mosher, D.C., Erbacher, J., Malone, M.J. (Eds.), Proceedings of the Ocean Drilling Program. Scientific Results, vol. 207. Ocean Drilling Program, College Station, TX, pp. 1–23.

Boyle, E.A., 1983. Manganese carbonate overgrowths on foraminifera tests. Geochimica et Cosmochimica Acta 47 (10), 1815–1819.

Bréhéret, J.G., Brumsack, H.-J., 2000. Barite concretions as evidence of pauses in sedimentation in the Marnes Bleues Formation of the Vocontian Basin (SE France). Sedimentary Geology 130 (3–4), 205–228.

Breit, G.N., Wanty, R.B., 1991. Vanadium accumulation in carbonaceous rocks. A review of geochemical controls during deposition and diagenesis. Chemical Geology 91 (1–2), 83–97.

Broecker, W.S., Peng, T.-H., 1982. Tracers in the Sea. Eldigio Press, Palisades, New York.

Brumsack, H.-J., 1980. Geochemistry of Cretaceous black shales from the Atlantic Ocean (DSDP Legs 11, 14, 36, and 41). Chemical Geology 31, 1–25.

Brumsack, H.-J., 1986. The inorganic geochemistry of Cretaceous black shales (DSDP Leg 41) in comparison to modern upwelling sediments from the Gulf of California. In: Summerhayes, C.P., Shackleton, N.J. (Eds.), North Atlantic Paleoocenography. Special Publication, vol. 21. Geological Society, London, pp. 447–462.

Brumsack, H.-J., 1988. Rezente, Corg-reiche Sedimente als Schlüssel zum Verständnis fossiler Schwarzschiefer. Habilitationsschrift, Georg-August Universität Göttingen, Germany.

Brumsack, H.-J., 1989. Geochemistry of recent TOC-rich sediments from the Gulf of California and the Black Sea. Geologische Rundschau 78 (3), 851–882.

Brumsack, H.-J., 2006. The trace metal content of recent organic carbon-rich sediments: implications for Cretaceous black shale formation. Palaeogeography, Palaeoceanography, Palaeoecology 232 (2–4), 344–361.

Brumsack, H.-J., Gieskes, J.M., 1983. Interstitial water trace-metal chemistry of laminated sediments from the Gulf of California, Mexico. Marine Chemistry 14 (1), 89–106.

Brumsack, H.-J., Heydemann, A., Kühn, V., Rachold, V., Usdowski, E., 1995. Geochemistry and mineralogy of Middle Aptian sediments from the Lower Saxony Basin, NW Germany. Neues Jahrbuch für Geologie und Paläontologie. Abhandlungen 196 (2), 235–255.

Brunner, B., Bernasconi, S.M., 2005. A revised isotope fractionation model for dissimilatory sulfate reduction in sulfate reducing bacteria. Geochimica et Cosmochimica Acta 69 (20), 4759–4771.

Calvert, S.E., Pedersen, T.F., 1993. Geochemistry of recent oxic and anoxic marine sediments: implications for the geological record. Marine Geology 113 (1–2), 67–88.

Canfield, D.E., Raiswell, R., Westrich, J.T., Reaves, C.M., Berner, R.A., 1986. The use of chromium reduction in the analysis of reduced inorganic sulfur in sediments and shale. Chemical Geology 54 (1–2), 149–155.

Church, T.M., Wohlgemuth, K., 1972. Marine barite saturation. Earth and Planetary Science Letters 15 (1), 35–44.

Cline, J.D., 1969. Sectrophotometric determination of hydrogen sulfide in natural waters. Limnology and Oceanography 14 (3), 454–458.

Crusius, J., Calvert, S., Pedersen, T., Sage, D., 1996. Rhenium and molybdenum enrichments in sediments as indicators of oxic, suboxic, and sulfidic conditions of deposition. Earth and Planetary Science Letters 145 (1–4), 66–78.

Dean, W.E., Arthur, M.A., 1989. Iron–sulfur–carbon-relationship in organic sequences, I. Cretaceous Western Interior Seaway. American Journal of Science 289 (6), 708–743.

Dymond, J., Suess, E., Lyle, M., 1992. Barium in deep-sea sediments: a geochemical proxy for paleoproductivity. Paleoceanography 7 (2), 163–181.

Eagle, M., Paytan, A., Arrigo, K.R., van Dijken, G., Murray, R.W., 2003. A comparison between excess barium and barite as indicators of carbon export. Paleoceanography 18 (1), 1021.

Emerson, S.R., Huested, S.S., 1991. Ocean anoxia and the concentrations of molybdenum and vanadium in seawater. Marine Chemistry 34 (3–4), 177–196.

Erbacher, J., Mosher, D.C., Malone, M.J., Shipboard Scientific Party, 2004. Proceedings of the Ocean Drilling Program. Initial Reports, vol. 207. Ocean Drilling Program, College Station, TX, p. 89.

Erbacher, J., Friedrich, O., Wilson, P.A., Birch, H., Mutterlose, J., 2005. Stable organic carbon isotope stratigraphy across Oceanic Anoxic Event 2 of Demerara Rise, Western Tropical Atlantic. Geochemistry, Geophysics, Geosystems 6, Q06010.

Forster, A., Schouten, S., Moriya, K., Wilson, P., Sinninghe Damsté, J.S., 2007. Tropical warming and intermittent cooling during the Cenomanian/Turonian oceanic anoxic event 2: sea surface temperature records from the equatorial Atlantic. Paleoceanography 22, PA1219.

Fossing, H., Jørgensen, B.B., 1989. Measurement of bacterial sulfate reduction in sediments. Evaluation of a single-step chromium reduction method. Biogeochemistry 8 (3), 205–222.

Friedrich, O., Erbacher, J., 2006. Benthic foraminiferal assemblages from Demerara Rise (ODP Leg 207, western tropical Atlantic): possible evidence for a progressive opening of the equatorial Atlantic gateway. Cretaceous Research 27 (3), 377–397.

Friedrich, O., Erbacher, J., Mutterlose, J., 2006. Paleoenvironmental changes across the Cenomanian/Turonian Boundary Event (Oceanic Anoxic Event 2) as indicated by benthic foraminifera from the Demerara Rise (ODP Leg 207). Revue de Micropaléontologie 49 (3), 121–139.

Gale, A.S., Jenkyns, H.C., Kennedy, W.J., Corfield, R.M., 1993. Chemostratigraphy versus biostratigraphy: data from around the Cenomanian–Turonian boundary. Journal of the Geological Society 150 (1), 29–32.

Galimov, E., 2006. Isotope organic geochemistry. In: Bouillon, S., Böttcher, M.E. (Eds.), Stable Isotopes in Biogeosciences. Organic Geochemistry, vol. 37(10), pp. 1200–1262.

Gauthier, D.L., 1987. Isotopic composition of pyrite: relationship to organic matter type and iron availability in some North American Cretaceous shales. Chemical Geology 65, 293–303.

Gendron, A., Silverberg, N., Sundby, B., Lebel, J., 1986. Early diagenesis of cadmium and cobalt in sediments of the Laurentian Trough. Geochimica et Cosmochimica Acta 50 (1), 741–747.

Gingele, F.X., Kasten, S., 1994. Solid-phase manganese in Southeast Atlantic sediments: Implications for the paleoenvironment. Marine Geology 121 (3–4), 317–332.

Hardas, P., Mutterlose, J., 2007. Calcareous nannofossil assemblages of Oceanic Anoxic Event 2 in the equatorial Atlantic: evidence of an eutrophication event. Marine Micropaleontology 66 (1), 52–69.

Hartmann, M., Nielsen, H., 1969. δ^{34}S-Werte in rezenten Meeressedimenten und ihre Deutung am Beispiel einiger Sedimentprofile aus der westlichen Ostsee. Geologische Rundschau 58 (2), 621–655.

Hatch, J.R., Leventhal, J.S., 1992. Relationship between inferred redox potential of the depositional environment and geochemistry of the Upper Pennsylvanian (Missourian) Stark Shale Member of the Dennis Limestone, Wabaunsee County, Kansas, USA. In: Meyers, P.A., Pratt, L.M., Nagy, B. (Eds.), Geochemistry of Metalliferous Black Shales. Chemical Geology, vol. 99(1–3), pp. 65–82.

Hebting, Y., Schaeffer, P., Behrens, A., Adam, P., Schmitt, G., Schneckenburger, P., Bernasconi, S.M., Albrecht, P., 2006. Biomarker evidence for a major preservation pathway of sedimentary organic carbon. Science 312 (5780), 1627–1631.

Heggie, D., Lewis, T., 1984. Cobalt in pore waters of marine sediments. Nature 311 (5985), 453–455.

Helly, J.J., Levin, L.A., 2004. Global distribution of naturally occurring marine hypoxia on continental margins. Deep-Sea Research Part I 51 (9), 1159–1168.

Helz, G.R., Miller, C.V., Charnock, J.M., Mosselmans, J.F.W., Pattrick, R.A.D., Garner, C.D., Vaughan, D.J., 1996. Mechanism of molybdenum removal from the sea and its concentration in black shales: EXAFS evidence. Geochimica et Cosmochimica Acta 60 (19), 3631–3642.

Hetzel, A., Brumsack, H.-J., Schnetger, B., Böttcher, M.E., 2006. Inorganic geochemical characterization of lithologic units recovered during ODP Leg 207 (Demerara Rise). In: Mosher, D.C., Erbacher, J., Malone, M.J. (Eds.), Proceedings of the Ocean Drilling Program, Scientific Results, 207. Ocean Drilling Program, College Station, TX, pp. 1–37.

Ingall, E.D., Bustin, R.M., Van Cappellen, P., 1993. Influence of water column anoxia on the burial and preservation of carbon and phosphorus in marine shales. Geochimica et Cosmochimica Acta 57 (2), 303–316.

Jacobs, L., Emerson, S., Skei, J., 1985. Partitioning and transport of metals across the O_2/H_2S interface in a permanently anoxic basin: Framvaren Fjord, Norway. Geochimica et Cosmochimica Acta 49 (6), 1433–1444.

Jacobs, L., Emerson, S., Huested, S.S., 1987. Trace metal geochemistry in the Cariaco Trench. Deep-Sea Research 34 (5–6), 965–981.

Kolonic, S., Sinninghe Damsté, J.S., Böttcher, M.E., Kuypers, M., Kuhnt, W., Beckmann, B., Scheeder, G., Wagner, T., 2002. Geochemical characterization of Cenomanian/Turonian Black Shales from the Tarfaya Basin (SW Morocco): relationships between palaeoenvironmental conditions and early sulphurization of sedimentary organic matter. Journal of Petroleum Geology 25 (3), 325–350.

Kuhnt, W., Herbin, J.P., Thurow, J., Wiedmann, J., 1990. Distribution of Cenomanian–Turonian organic facies in the Western Mediterranean and along the adjacent Atlantic margin. In: Huc, A.Y. (Ed.), Deposition of Organic Facies. AAPG Studies in Geology, vol. 30, pp. 133–160.

Kuypers, M.M.M., Pancost, R.D., Nijenhuis, I.A., Sinninghe Damsté, J.S., 2002. Enhanced productivity led to increased organic carbon burial in the euxinic North Atlantic basin during the late Cenomanian oceanic anoxic event. Paleoceanography 17 (4), 1051.

Lyons, T.W., Berner, R.A., 1992. Carbon–sulfur–iron systematics of the uppermost deep water sediments of the Black Sea. Chemical Geology 99 (1–3), 1–27.

Lyons, T.W., Severmann, S., 2006. A critical look at iron paleoredox proxies: new insights from modern euxinic marine basins. Geochimica et Cosmochimica Acta 70 (23), 5698–5722.

McManus, J., Berelson, W.M., Klinkhammer, G.P., Johnson, K.S., Coale, K.H., Anderson, R. F., Kumar, N., Burdige, D.J., Hammond, D.E., Brumsack, H.-J., McCorkle, D.C., Rushdi, A., 1998. Geochemistry of barium in marine sediments: implications for its use as a paleoproxy. Geochimica et Cosmochimica Acta 62 (21–22), 3453–3473.

Morford, J.L., Emerson, S.E., 1999. The geochemistry of redox sensitive trace metals in sediments. Geochimica et Cosmochimica Acta 63 (11–12), 1735–1750.

Mort, H.P., Adatte, T., Föllmi, K.B., Keller, G., Steinmann, P., Matera, V., Berner, Z., Stüben, D., 2007. Phosphorus and the roles of productivity and nutrient recycling during oceanic anoxic event 2. Geology 35 (6), 483–486.

Musavu-Moussavou, B., Danelian, T., 2006. The Radiolarian biotic response to Oceanic Anoxic Event 2 in the southern part of the Northern proto-Atlantic (Demerara Rise, ODP Leg 207). Revue de Micropaléontologie 49 (3), 141–163.

Nederbragt, A.J., Thurow, J., Vonhof, H., Brumsack, H.-J., 2004. Modelling oceanic carbon and phosphorus fluxes: implications for the cause of the late Cenomanian Oceanic Anoxic Event (OAE2). Journal of the Geological Society 161 (4), 721–728.

Nederbragt, A.J., Thurow, J., Pearce, R., 2007. Sediment composition and cyclicity in the mid-Cretaceous at Demerara Rise, ODP Leg 207. In: Mosher, D.C., Erbacher, J., Malone, M.J. (Eds.), Proceedings of the Ocean Drilling Program. Scientific Results, vol. 207. Ocean Drilling Program, College Station, TX, pp. 1–31.

Neretin, L.N., Böttcher, M.E., Jørgensen, B.B., Volkov, I.I., Lüschen, H., Hilgenfeldt, K., 2004. Pyritization processes and greigite formation in the advancing sulfidization front in the Upper Pleistocene sediments of the Black Sea. Geochimica et Cosmochimica Acta 68 (9), 2081–2093.

Neubert, N., Nägler, T., Böttcher, M.E., 2008. Sulfidity controls molybdenum isotope discrimination into euxinic sediments: evidence from the modern Black Sea. Geology 36 (10), 775–778.

Nijenhuis, I.A., Brumsack, H.-J., de Lange, G.J., 1998. The trace element budget of the eastern Mediterranean during Pliocene sapropel formation. In: Robertson, A.H.F., Emeis, K.-C., Richter, C., Camerlenghi, A. (Eds.), Proceedings of the Ocean Drilling Program. Scientific Results, vol. 160. Ocean Drilling Program, College Station, TX, pp. 199–206.

Passier, H.F., Bosch, H.-J., Nijenhuis, I.A., Lourens, L.J., Böttcher, M.E., Leenders, A., Damste, J.S.S., De Lange, G.J., De Leeuw, J.W., 1999a. Sulfidic Mediterranean surface waters during Pliocene sapropel formation. Nature 397 (6715), 146–149.

Passier, H.F., Böttcher, M.E., de Lange, G.J., 1999b. Sulfur enrichment in organic matter of eastern Mediterranean sapropels: a study of sulfur isotope partitioning. Aquatic Geochemistry 5 (1), 99–118.

Paytan, A., Kastner, M., Chavez, F.P., 1996. Glacial to interglacial fluctuations in productivity in the equatorial Pacific as indicated by marine barite. Science 274 (5291), 1355–1357.

Paytan, A., Mearon, S., Cobb, K., Kastner, M., 2002. Origin of marine barite deposits: Sr and S isotope characterization. Geology, 30 (8), 747–750.

Paytan, A., Kastner, M., Campbell, D., Thiemens, M.H., 2004. Seawater sulfur isotope fluctuations in the Cretaceous. Science 304 (5677), 1663–1665.

Piper, D.Z., 1994. Seawater as the source of minor elements in black shales, phosphorites and other sedimentary rocks. Chemical Geology 114 (1–2), 95–114.

Poulton, S.W., Raiswell, R., 2002. The low-temperature geochemical cycle of iron: from continental fluxes to marine sediment deposition. American Journal of Science 302 (9), 774–805.

Prakash Babu, C., Brumsack, H.-J., Schnetger, B., 1999. Distribution of organic carbon in surface sediments along the eastern Arabian Sea: a revisit. Marine Geology 162 (1), 91–103.

Raiswell, R., Canfield, D.E., 1998. Sources of iron for pyrite formation in marine sediments. American Journal of Science 298 (3), 219–245.

Redfield, A.C., 1958. The biological control of chemical factors in the environment. American Scientist 46, 205–221.

Schlanger, S.O., Jenkyns, H.C., 1976. Cretaceous oceanic anoxic events: causes and consequences. Geologie en Mijnbouw 55, 179–184.

Schlanger, S.O., Arthur, M.A., Jenkyns, H.C., Scholle, P.A., 1987. The Cenomanian–Turonian Oceanic Anoxic Event, I. Stratigraphy and distribution of organic carbon-rich beds and the marine δ^{13}C excursion. In: Brooks, J., Fleet, A.J. (Eds.), Marine Petroleum Source Rocks. Geological Society, London. Special Publication, vol. 26, pp. 371–399.

Schmitz, B., 1987. Barium, equatorial high productivity, and the northward wandering of the Indian continent. Paleoceanography 2 (1), 63–77.

Shipboard Scientific Party, 2004. Leg 207 summary. In: Erbacher, J., Mosher, D.C., Malone, M.J., et al. (Eds.), Proceedings of the Ocean Drilling Program. Initial Reports, vol. 207. Ocean Drilling Program, College Station, TX, pp. 1–89.

Strauss, H., 1999. Geological evolution from isotope proxy signals: sulfur. Chemical Geology 161 (1–3), 89–101.

Thurow, J., Brumsack, H.-J., Rullkötter, J., Littke, R., Meyers, P., 1992. The Cenomanian/Turonian boundary event in the Indian Ocean — a key to understand the global picture. In: Duncan, R.A., Rea, D.K., Kidd, R.B., von Rad, U., Weissel, J.K. (Eds.), The Indian Ocean: A Synthesis of Results from the Ocean Drilling Program. Geophysical Monograph, vol. 70. American Geophysical Union, pp. 253–273.

Torres, M.E., Brumsack, H.-J., Bohrmann, G., Emeis, K.C., 1996. Barite fronts in continental margin sediments: a new look at barium remobilization in the zone of sulfate reduction and formation of heavy barites in diagenetic fronts. Chemical Geology 127 (1–3), 125–139.

Tribovillard, N., Riboulleau, A., Lyons, T., Baudin, F., 2004. Enhanced trapping of molybdenum by sulfurized marine organic matter of marine origin in Mesozoic limestones and shales. Chemical Geology 213 (4), 385–401.

Tribovillard, N., Algeo, T.J., Lyons, T., Riboulleau, A., 2006. Trace metals as paleoredox and paleoproductivity proxies: an update. Chemical Geology 232 (1–2), 12–32.

van der Weijden, C.V., 2002. Pitfalls of normalization of marine geochemical data using a common divisor. Marine Geology 184 (3–4), 167–187.

Wanty, R.B., Goldhaber, M.B., 1992. Thermodynamics and kinetics of reactions involving vanadium in natural systems — accumulation of vanadium in sedimentary rocks. Geochimica et Cosmochimica Acta 56 (4), 1471–1483.

Wedepohl, K.H., 1971. Environmental influences on the chemical composition of shales and clays. In: Ahrens, L.H., Press, F., Runcorn, S.K., Urey, H.C. (Eds.), Physics and Chemistry of the Earth, vol. 8. Pergamon, Oxford, pp. 305–333.

Wedepohl, K.H., 1991. The composition of the upper earth's crust and the natural cycles of selected metals. Metals in natural raw materials. In: Merian, E. (Ed.), Metals and Their Compounds in the Environment. Natural Resources. VCH, Weinheim, pp. 3–17.

Werne, J.P., Hollander, D.J., Lyons, T.W., Sinninghe Damsté, J.S., 2004. Organic sulfur biogeochemistry: recent advances and future research directions. In: Amend, J.,

Edwards, K., Lyons, T. (Eds.), Sulfur Biogeochemistry: Past and Present. Special Paper, vol. 379. Geological Society of America, pp. 135–150.
Wijsman, J.W.M., Middelburg, J.J., Herrmann, P.M., Böttcher, M.E., Heip, C.H.R., 2001. Sulfur and iron speciation in surface sediments along the northwestern margin of the Black Sea. Marine Chemistry 74 (4), 261–278.
Wortmann, U.G., Chernyavsky, B., 2007. Effect of evaporite deposition on Early Cretaceous carbon and sulphur cycling. Nature 446 (7136), 654–656.
Wortmann, U.G., Bernasconi, S.M., Böttcher, M.E., 2001. Hypersulfidic deep biosphere indicates extreme sulfur isotope fractionation during single step microbial sulfate reduction. Geology 29 (7), 647–650.
Zhabina, N.N., Volkov, I.I., 1978. A method of determination of various sulfur compounds in sea sediments and rocks. In: Krumbein, W.E. (Ed.), Environmental Biogeochemistry and Geomicrobiology (vol. 3): Methods, Metals and Assessment. Ann Arbor Science Publications, pp. 735–745.